EuroGNC Navigation Guidance Control CEAS Bristol, UK June 11th-13th 2024
University of BRISTOL ROYAL AERONAUTICAL SOCIETY AIAA

Evaluation of the Indirect Ice Detection System Performance during the SENS4ICE Flight Test Campaigns

Christoph Deiler Scientific Advisor, DLR – German Aerospace Center, Institute of Flight Systems, 38108, Braunschweig, Germany. christoph.deiler@dlr.de

ABSTRACT

Supercooled large droplets (SLD) icing conditions have been the cause of severe aircraft accidents over the last decades. Existing countermeasures, even on modern airplanes, are not necessarily effective against the resulting ice formations, which raises a demand for reliable detection of SLD conditions for safe operations. The EU funded Horizon 2020 project SENS4ICE focused on new ice detection approaches and innovative sensor hybridization to target a fast and reliable SLD-ice detection. The performance-based (indirect) ice detection methodology is key to this approach and based on the changes of airplane flight characteristics under icing influence. This paper provides an overview on the development and implementation of the indirect ice detection (IID) algorithms in SENS4ICE. It provides and discusses exemplary results of the indirect ice detection system tests from the SENS4ICE flight test campaigns in North America (USA, February/March 2023) and Europe (France, April 2023).

Keywords: Aircraft Icing; Aircraft Flight Performance; Flight Data Analysis; Aircraft Flight Testing

Nomenclature

C_D	=	drag coefficient
C_{D0}	=	zero-lift drag coefficient
$\Delta C_{\tilde{D}}$	=	equivalent drag coefficient
C_L	=	lift coefficient
ΔISA	=	temperature offset to standard atmosphere, K
E	=	energy, J
$\dot{E}_{\text{tot}}$	=	energy change / power imbalance, W
$\dot{E}_{\text{tot,ref}}$	=	reference power imbalance, W
H	=	altitude, m
k_1, k_2	=	drag coefficient equation factors
LWC	=	liquid water content, g/m^3
m_{AC}	=	aircraft mass, kg
MVD	=	median volumetric diameter, microns
$\overline{q}$	=	dynamic pressure, Pa
S_{Wing}	=	wing surface area, m^2
V_{TAS}	=	true airspeed, m/s

α = angle of attack, rad

HIDS = hybrid ice detection system
IID = indirect ice detection
IPS = ice protection system
ref = reference
SLD = supercooled large droplets

1 Introduction

Icing can have hazardous effects on airplane performance characteristics and can be a limiting factor for the safe flight envelope. The change of the dynamic behavior and potential premature stall raise the need for pilot situational awareness and an adaption of control strategy. Different accidents worldwide have shown the criticality of icing related aircraft characteristics degradations, e.g., Refs. [1–4], especially when caused by supercooled large water droplets (SLD). Although in most cases the involved aircraft were equipped with state-of-the-art ice protection systems, the hazardous effects of SLD ice accretion led often to catastrophic events. These icing conditions can pose a high risk to the aircraft, crew and passengers, which requires specific detection and countermeasures to assure aircraft safety during flight. The certification of (modern) transport aircraft for flight into (known) icing conditions was mainly based on the certification requirements given in the so-called App. C to e.g., CS-25. But with the identified hazard to fixed-wing aircraft resulting from SLD the certification requirements were extended by the new App. O including SLD ice. From now on, manufacturers must prove that a newly developed airplane is also safe for flight into the even more hazardous SLD icing conditions. For flight safety it is now mandatory to detect the presence of SLD icing early. Furthermore, monitoring the aircraft's remaining capabilities during the further flight (in icing conditions) would give a relevant information to the pilots about the required adaption of operation, e.g., urgent need to enter masses with sufficiently warm temperatures to melt ice accretions on the airframe if the aerodynamics are significantly degraded. As a complicating fact, predicting the distinct change of aircraft characteristics caused by SLD ice formation is challenging and still a part of current aviation research. In addition, any reliable information about the current aircraft "icing state", i.e. the current aerodynamic degradation and abnormal flight characteristics, might be a base for flight control adaptation and hence automatic flight envelope protection as well as safe trajectory planning. This is not only relevant for manned aviation but also remotely piloted vehicles, today and in future.

Most of the existing ice protection systems (IPS) on transport aircraft require an significant amount of energy provided on board. Thermal ice protection systems of mainly commercial aircraft usually rely on bleed air, which reduces the engine effectiveness and increases fuel consumption of the engines. Using such a system preventively has a direct impact on fuel consumption and therefore aircraft emissions and operation cost. A more deliberate activation of the IPS can lead to more efficient but safe flight operations for which a reliable information about, e.g., the IPS effectiveness against the current icing encounter would be necessary. This information could be provided by suitable ice detection methods giving a hint about the presence of icing conditions, actual ice formation on the airframe and the effect on the flight characteristics [5, 6]. Moreover, it would also open possibilities for the modification of existing systems by modulating the thermal power according to the current need, directly reducing the energy consumption and increasing the aircraft efficiency.

The goal of the European Union Horizon 2020 Project "SENSors and certifiable hybrid architectures for safer aviation in ICing Environment" (SENS4ICE) project is to provide a more comprehensive overview on the icing conditions, ice formation and aircraft degradation status including the aircraft's remaining capabilities (icing-related change in aircraft flight physics, i.e., degraded aircraft performance) [7, 8]. Within SENS4ICE the "indirect ice detection" (IID) was further developed and matured and is one

Fig. 1 Embraer Phenom 300 flight test bench: prototype aircraft with all modification for the SENS4ICE North America flight test campaign; credit Embraer.

Fig. 2 Safire ATR 42-320 flight test bench (MSN 78): aircraft with all modification for the SENS4ICE European flight test campaign at Toulouse/Francazal airport; credit DLR/Safire.

important project pillar [6]. It is a novel methodology and system for the on-board surveillance of aircraft flight performance used for ice detection purposes and was originally formulated and presented as a performance-based ice detection methodology, e.g., in Ref. [5], being already under patent protection in several countries[9]. It utilizes the effect of aircraft performance degradation due to ice accretion on the airframe resulting in a change of aerodynamics, which was previously investigated in, e.g., Refs. [10–13]. The idea of the IID is not restricted to an application on large transport aircraft but can also enable a reliable ice detection for aircraft systems, such as small UAV, which currently have no ice detection system but operate in hazardous environments with very different icing conditions. The SENS4ICE project contained two major icing flight test campaigns: the North America campaign using an Embraer Phenom 300 prototype aircraft (see Fig. 1) and the European campaign with an ATR 42-320 (see Fig. 2) operated by SAFIRE [8, 14]. This paper contains first evaluation results from the North America fight test campaign conducted between February 22nd and March 10 2023 out of St. Louis Regional Airport (Alton, IL, USA) and the European fight test campaign conducted in April 2023 out of Toulouse (France) with a focus on the IID ability to reliably detect the performance degradation caused by different icing during several example ice events.

This paper is structured as follows:

- the SENS4ICE approach for a more comprehensive view on the aircraft icing situation to enhance flight safety is presented in section 2;

- a brief description of the indirect ice detection methodology based on the observed aircraft flight performance variation and the specific implementation of the detection algorithm for the SENS4ICE purpose are given in section 3 & 4;
- exemplary flight test data analysis from SENS4ICE icing flight test campaigns reflecting the system performance with regard to the ability of reliable ice detection in section 5.

Finally, a summary with initial conclusions are given in section 6.

2 A Comprehensive View on Aircraft Icing Situation: The SENS4ICE Approach

Since the 1990s accident analysis revealed the criticality of SLD-icing events for aviation safety, which forces the regulators to issue new certification requirements, e.g. in the App. O to CS-25 (EASA) or FAR Part 25 (FAA). But for certain aircraft types - mainly related to their size, design and operational profile - icing caused by smaller drops can also degrade the flight characteristics if the conditions encountered consist a large water content leading to large and fast accumulation of ice on the aircraft, classified as severe icing. Hence, although the atmospheric icing conditions cause different ice accumulation on the airframe, the major risk for aviation safety is the aerodynamic degradation, which is only dependent on the size and location of ice accumulation. In addition, also the severity in terms of e.g., ice accumulation rate, is no comprehensive indication of the real risk to the ongoing aircraft operation, if ice is only forming on unprotected surfaces not causing a significant degradation. Anyway, merging all the information available gives the most comprehensive view on the current icing situation, the aircraft condition and remaining safe operational capabilities. This is one main focus of the SENS4ICE detection approach to hybridize the sensing and support pilots to make one decision on the flight procedures required for the current icing situation and the dealing with especially supercooled large droplets.

In a layered approach a hybrid ice detection system (HIDS) is forming the core function accompanied by additional new nowcasting and enhanced weather forecasting. The latter allows to initially prevent the flight through hazardous icing conditions from a strategic and tactical point of view, whereas the hybrid detection architecture provides the necessary information to the flight crew for the IPS activation and the execution of safe exit strategies, when required. It combines in-situ measurement from various ice detection sensor technologies based on different physical principles (optical or remote sensing and ice accretion detection) with an indirect detection methodology. Hence, the HIDS allows to give a more general overview on the current aircraft icing than an individual system alone. In addition, the indirect detection methodology monitoring the current aircraft flight characteristic reveals the degraded aircraft flight envelope, which is essential for loss of control prevention. For example, work on the benefit of a safe flight envelope detection was done in, e.g., Ref. [15] with a different focus and approach but with noticeable results on the crew's situational awareness.

An overview on the layered safety concept is given in Fig. 3. The concept targets a general application and safety enhancement for fixed-wing aircraft icing and is not only dedicated to aircraft already certified for flight into known icing conditions (App. C). It intentionally goes beyond current certified aircraft systems proving safe operations in icing conditions.

The inner layer of the SENS4ICE safety concept in Fig. 3 focuses on the detection of the (remaining) safe flight envelope. This is at first independent of the icing conditions and includes a prediction of the current aircraft flight performance compromised by ice accretion which is directly related to the aerodynamic degradation. It is assumed that for safe flight operations an information about the current flight performance and aerodynamic degradation is more beneficial than a sole direct detection of potential icing conditions in flight without any further interpretation. The latter only allows to conclude on the need to leave the conditions or the ability to maintain but does not support the pilots in any other way during the

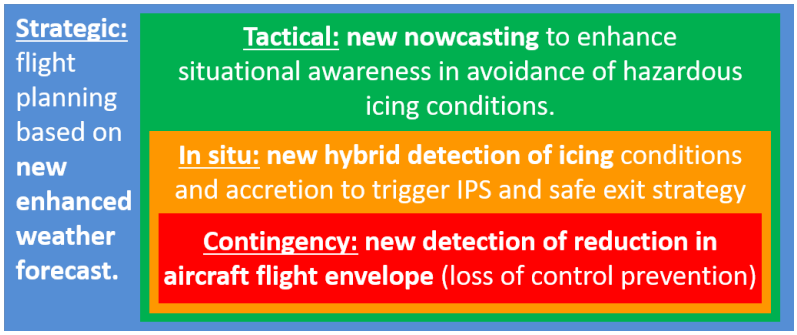

Fig. 3 SENS4ICE layered safety concept

further operation. Hence, the SENS4ICE hybridization combines the two different but complementary approaches of direct sensing – atmospheric icing conditions and ice accretion on specific surfaces – and indirect ice detection through predicting the degraded aircraft flight characteristics. There are several potential aircraft icing states which are not indicated correctly by a sole system. For example, when the aircraft enters icing conditions, accretion sensors and the IID do not directly indicate ice formation or a performance loss, whereas sensors monitoring the surrounding air will give a first indication of icing. But when the aircraft has ice on the airframe and leave the icing conditions, the atmospheric sensor technologies will not give an indication whereas accretion based sensors or the IID might correctly announce icing. Furthermore, when the ice is also removed from the accretion sensor surface, there might be still some ice formation present on the airframe (protected and/or unprotected surface) which will then only be indicated by the IID if the aerodynamic degradation is significant. Hence, this simple example shows why the SENS4ICE hybrid approach might be key to safe aircraft operation in a wider icing envelope.

For safe aircraft operation in icing conditions the most relevant question is about the potential degradation of aerodynamics with ice accretion present. If icing is present and also correctly announced by direct sensors, the flight performance and aircraft characteristics might not be degraded. Hence, if ice formation on the airframe has no adverse effects, and pilots are aware of the situation there is no need to take any actions to maintain safe operations. These would be only required if a degrading effect on aerodynamics is detected. With this envelope opening, operations in icing conditions could be enhanced and there is a potential for a wider icing certification.

3 Airframe Ice Detection through Flight Performance Monitoring

One major effect of aircraft ice accretion is a significant drag increase due to surface roughness changes, parasitic influence of ice formations, and local flow separation. Another effect of icing is a change of the aircraft lift behavior, causing e.g., earlier or more abrupt flow detachment with increasing angle of attack and/or a reduction in aircraft lift slope. Both together significantly alter the aircraft flight performance which can be monitored during flight. Figure 4 illustrates the typical icing-induced change of the lift and drag curves as generally described, e.g., in the AGARD report 344 [16]. Icing will also change the aircraft's flight dynamics (e.g., pitching and rolling moment), but these are not as specific as the general impact on lift and drag. Furthermore, the control characteristics are negatively affected by icing and change the aircraft behavior differently according to the specific occurrence of ice accretion. As these changes are very difficult to detect during flight, the IID relies on the icing related change of aircraft flight performance [5, 6].

Aircraft flight performance monitoring can provide crucial information to the pilots about the current (limited/degraded) aircraft capabilities while only requiring the sensor information already available on all modern airliners and business jets. The advantage of the developed methodology is that it relies only

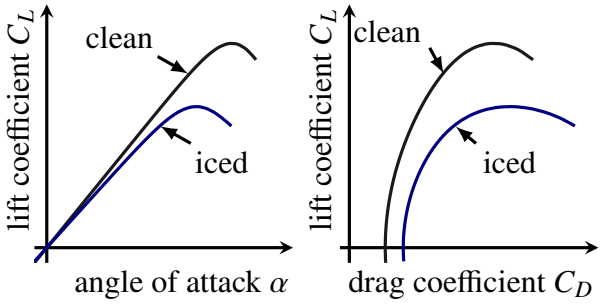

Fig. 4 Expected icing influence on aircraft aerodynamics (lift and drag coefficient); adapted from [16]

on the change in flight performance (i.e., steady flight states) contrary to the many failed attempts (e.g., in Refs. [17–22]) based on the estimation of changes in the aircraft's dynamic behavior or a combination of both. The change/degradation in the flight performance is an indicator of ice accretion that is both robust and highly available: unlike the approaches based on the detection of changes in the aircraft dynamical behavior, it can be used also during steady flight conditions (most of an operating flight) and can detect icing effects significantly before entering into stall. It is important to highlight that the method within the IID is focused on the flight performance changes with no need of any additional dynamic aircraft excitation. Such an excitation is not acceptable during normal operations as stated in Ref. [19] and especially not when flying with an aircraft that has a reduced (unknown) maximum-lift angle of attack due to icing.

The basic assumption for the indirect ice detection using performance monitoring is possibility to discriminate between (very slow and small) performance variation of a single aircraft over lifetime in service (or within a fleet of same type) and the (much faster) performance variation caused by icing. Factors causing the flight performance variations across airplanes from the same type are, for example, production tolerances, aircraft skin repairs, aircraft skin contamination (e.g., dirt), engine aging causing reduced efficiency, or engine contamination. The aircraft flight performance can be seen as follows:

$$\begin{aligned}\textbf{Flight Performance} = \;& \text{Nominal Aircraft Performance} \\ & + \text{Expectable Variation} \\ & + \textit{Variation to be detected}\end{aligned}$$

whereby the "Expectable Variation" part gathers the effects mentioned previously and the "*Variation to be detected*" is subject to the indirect (performance-based) ice detection approach. The first step is to determine the typical and most extreme flight performance variation ("Expectable Variation") encountered during regular airline operations (due to a real performance variation or sensor errors). This was done in a basic evaluation of airline operational flight data in Refs. [5, 23] to initially verify the feasibility of the approach. For the SENS4ICE flight test benches, similar analysis had been conducted on less data but with more "in-sight" knowledge about the aircraft types due to the involvement of the manufactures in the IID development. The results of this analysis are given in Refs.[24–26] for both flight test platforms. The measured performance variation of each aircraft indicated that the average variation in normal flight is below the expected influence of airframe ice accretion on flight performance (using the available test data). It can be furthermore reliably assumed that the variation above the 90% quantile (of data analyzed) results from the external influence which can be ignored for the ice detection and circumvented (e.g., for large scale atmospheric disturbances or dynamic maneuvers) or filtered (e.g., for measurement noise) within the designed algorithm. This was the successful first step for the further IID development within SENS4ICE.

The basic idea of the performance-based ice detection method is to compare the current (possibly ice-influenced) aircraft flight performance characteristics with a known reference (see Fig. 5). The flight

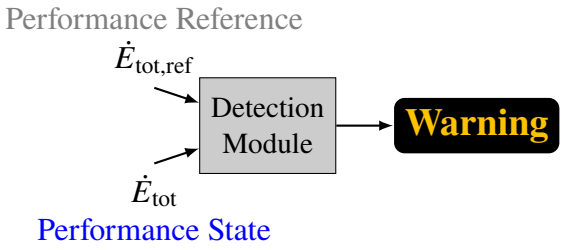

Fig. 5 Basic principle of the IID method based on the aircraft power imbalance in Equation (1); from [5]

performance can be defined as a power imbalance (change of total energy) $\dot{E}_{tot}$ for the current state and the reference, which allows representing the change of aircraft characteristics in a sole value. Consequently, this reduces the complexity of the detection algorithm. It further combines the individual parts of the aircraft performance related to aerodynamics and engines in a single observation. The power imbalance $\dot{E}_{tot}$ can be formulated as

$$\dot{E}_{\text{tot}} = V_{\text{TAS}} \cdot \dot{V}_{\text{TAS}} \cdot m_{\text{AC}} + \frac{1}{2} \cdot V_{\text{TAS}}^2 \cdot \dot{m}_{\text{AC}} + g \cdot \dot{H} \cdot m_{\text{AC}} + g \cdot H \cdot \dot{m}_{\text{AC}} \,, \tag{1}$$

with the altitude change (with respect to time) $\dot{H}$ referenced to the surrounding air, the speed change (with respect to time) $\dot{V}_{\text{TAS}}$ and the change of aircraft mass $\dot{m}_{\text{AC}}$ corresponding to the aircraft fuel consumption. Note that the gravitational acceleration is assumed to be constant and its variation with time can be neglected for the calculation of the power imbalance. To convert the power imbalance into an equivalent drag coefficient variation, which is more easy to assess from an engineering point of view, the formulation from [5] is used:

$$\Delta C_{\widetilde{D}} \approx \frac{\dot{E}_{\text{tot,ref}} - \dot{E}_{\text{tot}}}{V_{\text{TAS}} \cdot \overline{q} \cdot S_{\text{Wing}}} \tag{2}$$

This non-dimensional equivalent drag coefficient is calculated by comparison of the current determined power imbalance $\dot{E}_{\text{tot}}$ and a predefined reference value $\dot{E}_{\text{tot,ref}}$. The performance reference value is a function of the aircraft flight state defined by parameters like altitude, speed and load factor, and also the aircraft configuration (e.g., mass, high lift system configuration) and propulsion system state. If required, some corrections for additional influences, e.g., flight with side slip condition could be applied[5]. Furthermore, the airspeed V_{TAS} is derived from several measurements and contains a combination of aircraft flight path velocity and wind speed (both to be understood as 3D vectors). For the time derivative $\dot{V}_{\text{TAS}}$ the component related to the change of wind vector should be ignored in order to prevent it from falsifying the performance estimate. A variable wind-corrected energy change $\dot{E}_{\text{tot,corr}}$ could then be used changing $\dot{V}_{\text{TAS}}$ in Eq. (1) to $\dot{V}_{\text{TAS},\dot{\vec{V}}_{\text{k}}}$ considering only the airspeed change related to the flight path.

The equivalent drag coefficient is well comparable to a predefined threshold value and indicates an abnormal performance variation when exceeding. This is further independent from any flight point. Note that a drag coefficient value is well interpretable in terms of aerodynamics and flight mechanics by aerospace engineers and allows a direct assessment of the magnitude of aerodynamic degradation caused by icing. Within the IID, this drag coefficient is normalized with the aircraft's zero-lift drag coefficient and compared to a predefined threshold. Note that the choice for the representation of the performance reference is also dependent on the requirement for adaptation to a specific aircraft. Further detailed information on performance-based ice detection, which is already under patent protection in several countries[9], can be found in [5].

4 Implementation of the Indirect Ice Detection Algorithm

The indirect ice detection is implemented as a modular set of functions, including the core detection algorithm, the required data preprocessing and a subsequent detection result filtering to prevent false detections. The latter also guarantees the necessary system robustness and consequently reliability. Within SENS4ICE, the indirect ice detection is part of the HIDS and allows with its specific implementation detecting performance degradations and therefore the ice accretion (see Fig. 6). The HIDS implementation was designed to be applicable to SENS4ICE flight test campaigns with the very different aircraft configurations: a light business jet aircraft (Embraer Phenom 300) and a regional class turbo-prop aircraft (ATR 42). This applicability was possible through the generic formulation of the detection methodology itself, not relying on specific information about the aircraft: the required aircraft-specific adaption of the detection was achieved by considering the aircraft-specific reference, which is an input to the algorithm and not part of the core implementation. There are several needs for adjustments inside the IID for a specific aircraft type, mainly as part of the "Aircraft Flight Data" and "Performance Reference Data Base" blocks in Fig. 6:

- flight data preprocessing,
- flight performance reference data base,
- indirect ice detection threshold and confirmation times, and
- detection reliability conditions.

A detailed description about these required adjustments is given in Ref. [6]. The flight performance reference, the detection threshold and confirmation times are briefly described below. For the SENS4ICE flight testing, the IID was implemented in MATLAB/Simulink by DLR and integrated in the HIDS developed by Safran Aerosystems. Hence, it had to be embedded in the corresponding real time software on the dSpace MicroAutoBox for the flight tests. More details about the implementation of the HIDS and IID algorithms are given in the corresponding final SENS4ICE project report [27].

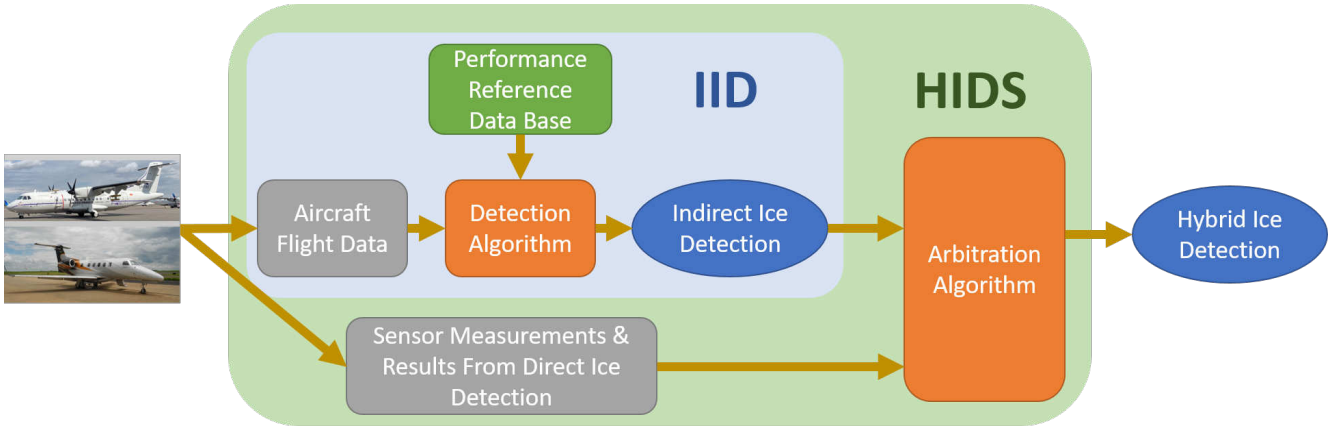

Fig. 6 Visualization of HIDS concept used within SENS4ICE (pictures credit DLR / Embraer / SAFIRE).

4.1 Flight Performance Reference Data Base

The IID relies on an accurate flight performance reference which allows to compute the current flight performance to be compared to the measured one within the detection module. A simple way for the definition of the aircraft flight performance reference is the usage of a multi-dimensional table [5, 6]. Another way is to calculate the reference power imbalance from an aerodynamic data base and engine thrust model, if both are available. In such cases it must be determined if the variation in the reference power imbalance results from changes of the aircraft aerodynamics or the engine performance. For the implementation in SENS4ICE an engine thrust model was available and the reference power imbalance can be formulated as a function of flight condition, aircraft configurations (using a reference

aerodynamic model representation) and the current predicted engine thrust. Having this separation with an individual aerodynamic reference model, it was possible to adapt the reference aerodynamics to the specific conditions given by the flight test benches having several external probes attached to the test aircraft influencing the aircraft's flight performance. Also, the performance reference was continuously checked during the flight test campaign to monitor its validity. As presented in Ref. [25], a post-campaign adaption for the Phenom 300 prototype engine thrust reference was required, which could be easily done due to the present separation of aerodynamics and thrust. Note that this was mainly relevant for the test configuration within the SENS4ICE project and might be different for a potential operational IID implementation in future.

Within the IID implementation a linear parameter extension of the drag polar representation was already foreseen allowing the adaptation of the aircraft aerodynamics to the SENS4ICE aircraft modifications:

$$C_D = \left(C_{D0,\mathrm{ref}} + \Delta C_{D0}\right) + \left(k_{1,\mathrm{ref}} + \Delta k_1\right) \cdot C_L + \left(k_{2,\mathrm{ref}} + \Delta k_2\right) \cdot C_L^2 \,. \tag{3}$$

Figure 7 shows the drag polar calculated from flight test data of several clean air flights with the Phenom 300 prototype in campaign configuration together with the pre-campaign reference used to design the IID and the modified drag polar used for the icing flight tests [25]. A similar plot for the ATR 42 flight test bench is given in Fig. 8 [26]. In both cases it is clearly visible that the SENS4ICE configuration containing the required modifications for the additional probes on the aircraft significantly increases the drag and consequently decreases the flight performance in reference conditions. For a valid result of the IID testing during the icing campaign flights, the new campaign reference for both aircraft was essential. Note that the flight performance reference in SENS4ICE is based on certain a priori knowledge and information obtained from a specific flight data evaluation. But for new aircraft designs it could also be on the design models and initial prototype flight test results.

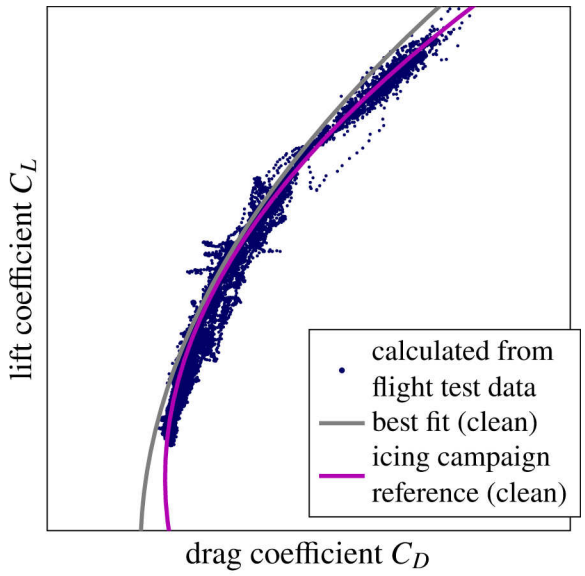

Fig. 7 Aircraft drag polar for Phenom 300 prototype used for the SENS4ICE North America icing flight test campaign: calculated lift and drag coefficient from flight test data (blue dots), pre-campaign reference drag polar (gray line, no SENS4ICE aircraft modification) and adapted campaign reference drag polar considering aircraft modifications (magenta line); clean air flight test data with aircraft in final configuration with all modification required for SENS4ICE in February 2023; from [25]

4.2 Detection Threshold, Confirmation Time and Reliability Conditions

A detection threshold on the equivalent drag coefficient is defined to reveal the abnormal flight performance caused by icing. For practical reasons, the detection is not done on the absolute value of the

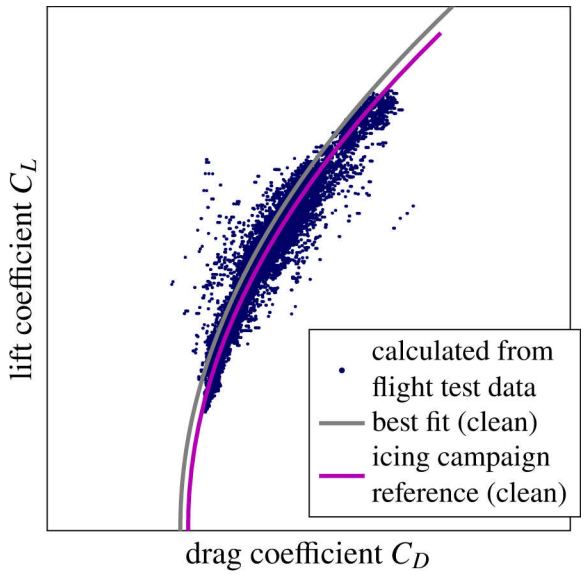

Fig. 8 Aircraft drag polar for Safire ATR 42-320 (MSN78) used for the SENS4ICE European icing flight test campaign: calculated lift and drag coefficient from flight test data (blue dots), pre-campaign reference drag polar (gray line, no SENS4ICE aircraft modification) and adapted campaign reference drag polar considering aircraft modifications (magenta line); clean air flights in final aircraft configuration with all modification required for SENS4ICE on March 22nd and 23rd, 2023; from [26]

equivalent drag increase but on a relative value with the zero-lift drag coefficient as base. In a nominal case, the additional drag coefficient is zero and there is no relative change to the normal drag condition. During normal operation flight there is a constant fluctuation of measured flight performance, which have to be considered by the detection algorithm through providing a suitable low-pass filtering function. In addition, the implementation of a confirmation time allows to further prevent false alarms cause by short-time threshold exceeding if set large enough. The confirmation time is chosen in accordance with the modeling accuracy of the whole IID system chain and quality of flight data, where high quality and accuracy of flight data measurements can lead to relatively short confirmation times and vice versa. For the detection, the confirmation time frame is chosen relatively short to ensure fast response behavior but for reset that confirmation time must be much longer to guarantee the threshold is reliably undershot and the icing-related performance degradation is not present anymore. The corresponding values are given in Table 1. The IID is designed to run continuously during the whole flight and to monitor the aircraft flight performance, and a potential degradation, independently from any specific flight phase or maneuver, as discussed in Ref. [5]. The SENS4ICE implementation is experimental and therefore limited to one aircraft specific configuration defined for the flight test in icing conditions. Hence, other aircraft configurations will be detected and the IID is designed to freeze and set an unreliability flag allowing the HIDS to discard the current IID output. A more detailed description is given in Ref. [6].

5 Exemplary Results from SENS4ICE Flight Test Campaigns

This paper presents initial results from specific flights of the North America and European icing flight test campaigns. Preliminary results from other flights of both campaigns are presented in Refs. [25, 26] in a similar way.

5.1 Example from North America flight test campaign

The example flight left St. Louis Regional Airport in Alton, Illinois, on February 25th, 2023, in a north easterly direction to the great lakes at 11:38 UTC (5:38 local) reaching Eugene F. Kranz Toledo

	Safire ATR 42-320	Phenom 300 prototype
detection threshold (for flight test)	15 %	10 %
detection threshold (post-campaign)	10 %	
confirmation time frame for detection (threshold exceeded more than 50%)	20 s	
confirmation time for reset (threshold undershot more than 50%)	180 s	

Table 1 Detection threshold values (relative drag coefficient increase) and confirmation time for the IID implementation.

Express Airport in Toledo, Ohio, at 13:42 UTC (7:42 local). Within the vicinity of the great lakes after around 40 min of flight icing conditions were found leading to five successful encounters also including supercooled large droplet icing conditions, as defined in App. O. Note that during the encounters the total amount of SLD was small compared to the other supercooled water drops with lower size, as it was expected due to the rarity of SLD in the atmosphere. An overview of the flight is given in Fig. 9 including the flight track and icing encounters.

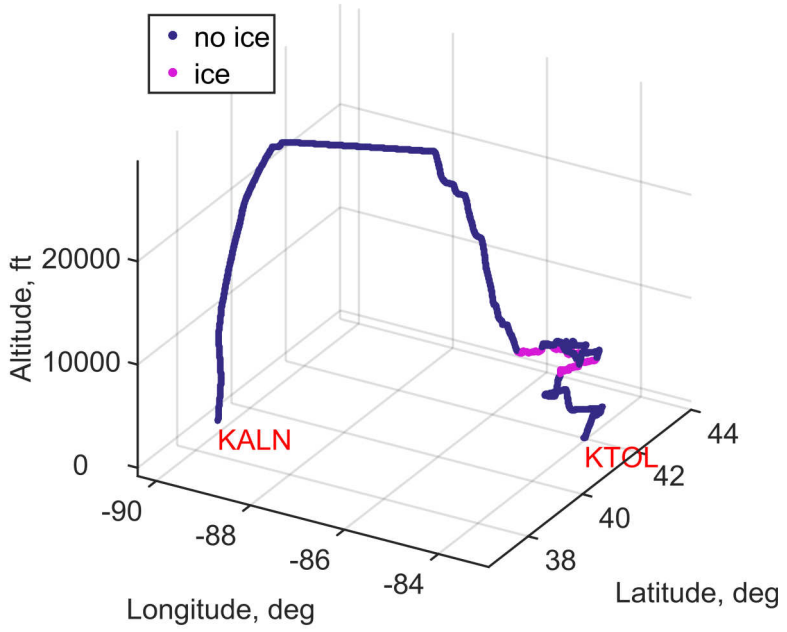

Fig. 9 Flight track from SENS4ICE North America icing campaign flight on February 25rd, 2023 (St. Louis Regional Airport, KALN, to Eugene F. Kranz Toledo Express Airport, KTOL): geodetic position and altitude with indication of icing encountered.

Two important remarks must be made in order to further evaluate the IID results:

1) The overall liquid water content was relatively low during these presented encounters in the presented flight with a different droplet distribution compared to the results presented in Ref. [25] for a smaller droplet case. This has a direct effect on the visible performance degradation during the encounters which is successfully detected by the IID. The maximum values reached after a comparable time in icing conditions (up to 7min) are lower because less ice was gathered in total on the aircraft, which is mainly related to the total amount of water drops collected. Note that this

does not imply any severity, criticality or safety evaluation for the aircraft or flight operation, but basically is required as background knowledge to interpret the IID results during the encounters including SLD.

2) The presence of SLD in the clouds which then cause icing on the aircraft when flown through does not directly imply a change of the ice accretion on the airframe. For the ice formation and the resulting shapes affecting the aircraft's aerodynamics the total amount of SLDs in relation smaller droplets is important. A few SLDs in the clouds with a total amount of smaller drops several magnitudes larger might not affect the resulting ice formation whereas, the presence of a majority of SLD in the icing conditions will of course strongly affect the appearance of ice shapes on the aircraft. Hence, the IID results for this flight, which only encountered a very small amount of SLD in the conditions, are not consequently representative for an expectable performance degradation as it could result from App. O conditions with a larger amount of SLD. For the IID and the performance degradation the negative impact of ice shapes on aerodynamics is important and this could be similar or worse when caused solely be classical App. C conditions than for the conditions encountered also including SLD. Furthermore, every encounter is different, so it is per se very difficult to compare the specific results in order to make general conclusions.

5.1.1 Indirect ice detection system performance during North America campaign flight

The IID performance during this example is evaluated for the five icing encounters at the end of the flight near Toledo, Ohio. These are visualized as time history plots in Figs. 10 to 15. Figure 10 contains the whole flight as overview and Figs. 11 to 15 the individual encounters. The top plot contains the altitude and indicated airspeed in which it is clearly visible that the aircraft was intentionally descending into the (expected) icing conditions (after 12:15 UTC) with reducing the airspeed and climbing again out of these together with increasing the airspeed after a certain encounter time. The second plot (from top) shows the relative drag coefficient (based on clean aircraft zero-lift drag) and gives a direct impression about the performance degradation. In parallel the IID detection output is given allowing a direct comparison of drag increase and IID detection performance. Note that the shown data are results of the replayed IID calculation directly fed with aircraft data/measurements including the post-campaign modified engine model described in [25]. There is no significant difference in the IID code implementation between the desktop replay and the flight test implementation within the HIDS (dSpace box) except for the used/adjusted engine thrust model. The third plot (from top) contains the information about the encountered icing conditions. The measured droplet size (MVD) and liquid water content (LWC) describe the atmospheric icing conditions, in the presented case including supercooled large droplets (SLDs). The dashed lines indicate their portion whereas the solid lines contain all droplets (including smaller sizes). The bottom plot contains the measured static air temperature as well as the averaged engine fan speed (left and right right, assuming symmetric thrust conditions). During the descent into the icing conditions the temperature decreases significantly and increases again after leaving the conditions, indicating an atmospheric inversion layer. This allows a direct assessment about the icing encountered leading to airframe ice accretion and hence a performance degradation, together with the possibility to cross-check the detection reset with the flight through warm air and consequently de-icing. The averaged engine fan speed is directly linked to the total engine thrust and therefore gives an information about the forces applied to the aircraft in combination with the aerodynamic performance degradation.

During all encounters of this flight the IID was able to reliably detect the performance degradation 2 minutes or less after the ice build-up started. The confirmed detection remained every time until the aircraft left the conditions and was completely de-iced again. For these encounters, the time to restore the nominal flight performance and to reset the detection flag took approximately the same time as the aircraft stayed in the conditions itself. This shows the great value of the IID because it reliably indicates the aircraft degradation being eventually critical for the aircraft operation if it is unknown whether the

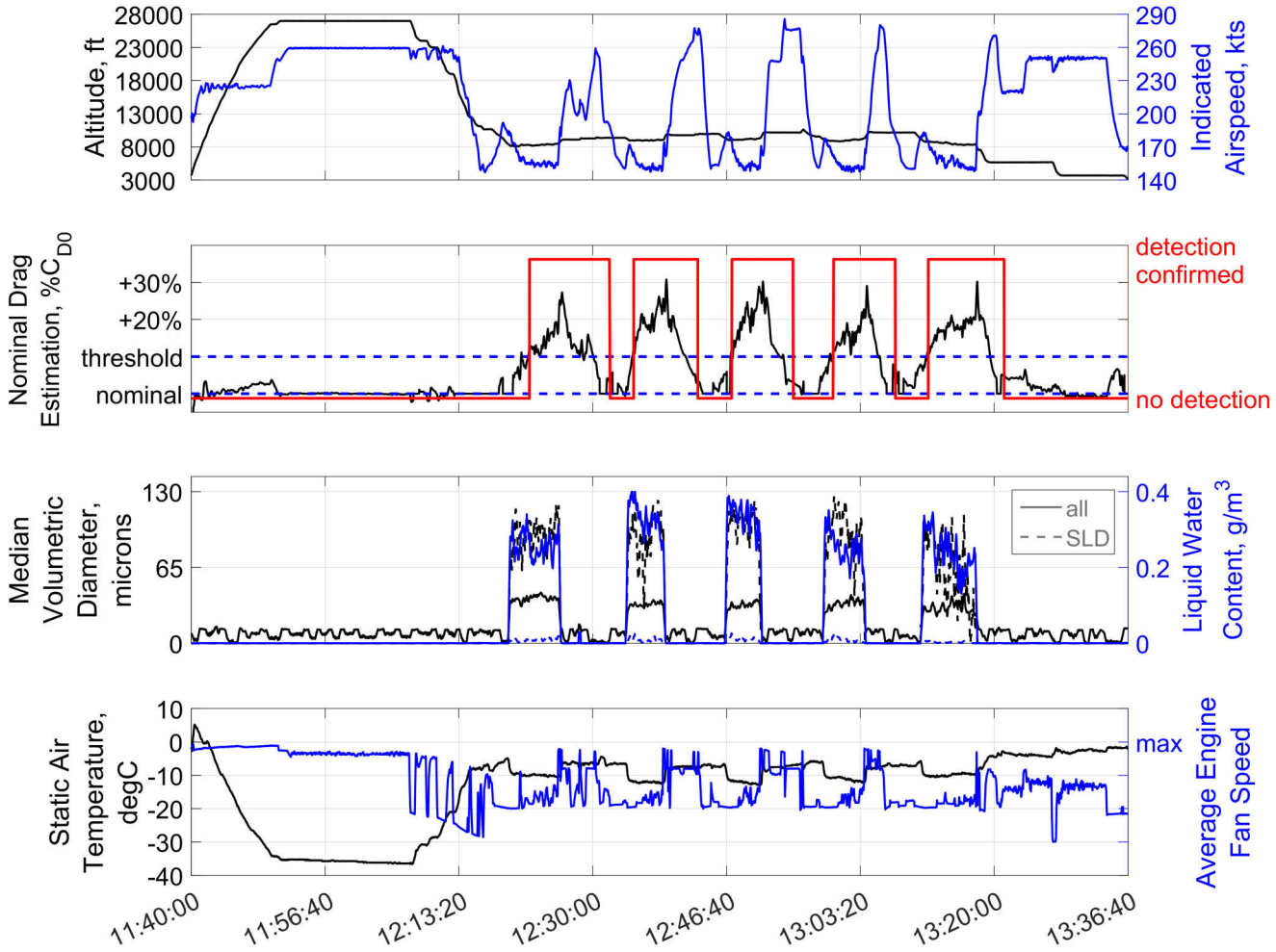

Fig. 10 Time history of IID system performance during example flight on February 25rd, 2023 (11:40:00 UTC to 13:36:40 UTC): altitude and indicated airspeed (top), relative drag coefficient and IID detection output (second plot), and MVD and LWC of encountered icing conditions including SLD portion (dashed lines) (third plot), and static air temperature and average engine fan speed (bottom); detection threshold at 10 % relative drag increase and adjusted engine thrust model behavior.

icing conditions have even already been left. This is one of the keys related to the layered safety concept provided by SENS4ICE including the HIDS approach.

Figure 11 contains an extract of the first encounter (from 12:19 UTC to 12:33 UTC) with SLD icing conditions present between around 12:19:30 UTC until 12:26 UTC. The aircraft descended in icing conditions and light ice was accumulated on the unprotected surfaces[1] resulting in a continuous increase of estimated drag exceeding the threshold at 12:22 UTC until the end of the encounter estimated drag increased around 20% (relative increase normalized with zero lift drag) above nominal. For leaving the cloud layer and icing conditions full thrust was applied to climb and accelerate. As briefly discussed above and detailed in Ref. [25] the engine thrust model used for SENS4ICE showed some deficiencies which mostly could be reduced by a post-flight model modification. Nevertheless, some residuals of engine thrust model mismatch compared to true thrust behavior are still present resulting in a further estimated drag increase correlated to full thrust conditions during the climb out. But this has no direct impact on the IID evaluation or overall results presented here. To clean the aircraft from the accreted ice several minutes of flight in warmer air outside the icing conditions with higher speed was required. After the nominal performance was restored around 12:31:50 UTC the IID ice detection output was reset. Note

[1]according to Embraer flight test engineer's observation during flight

that data extract also contained flight with spoiler extended, where the IID is per default set to stop its operation and output nominal flight performance without any drag increase, which is shown in Fig. 11 by the flat line in estimated drag.

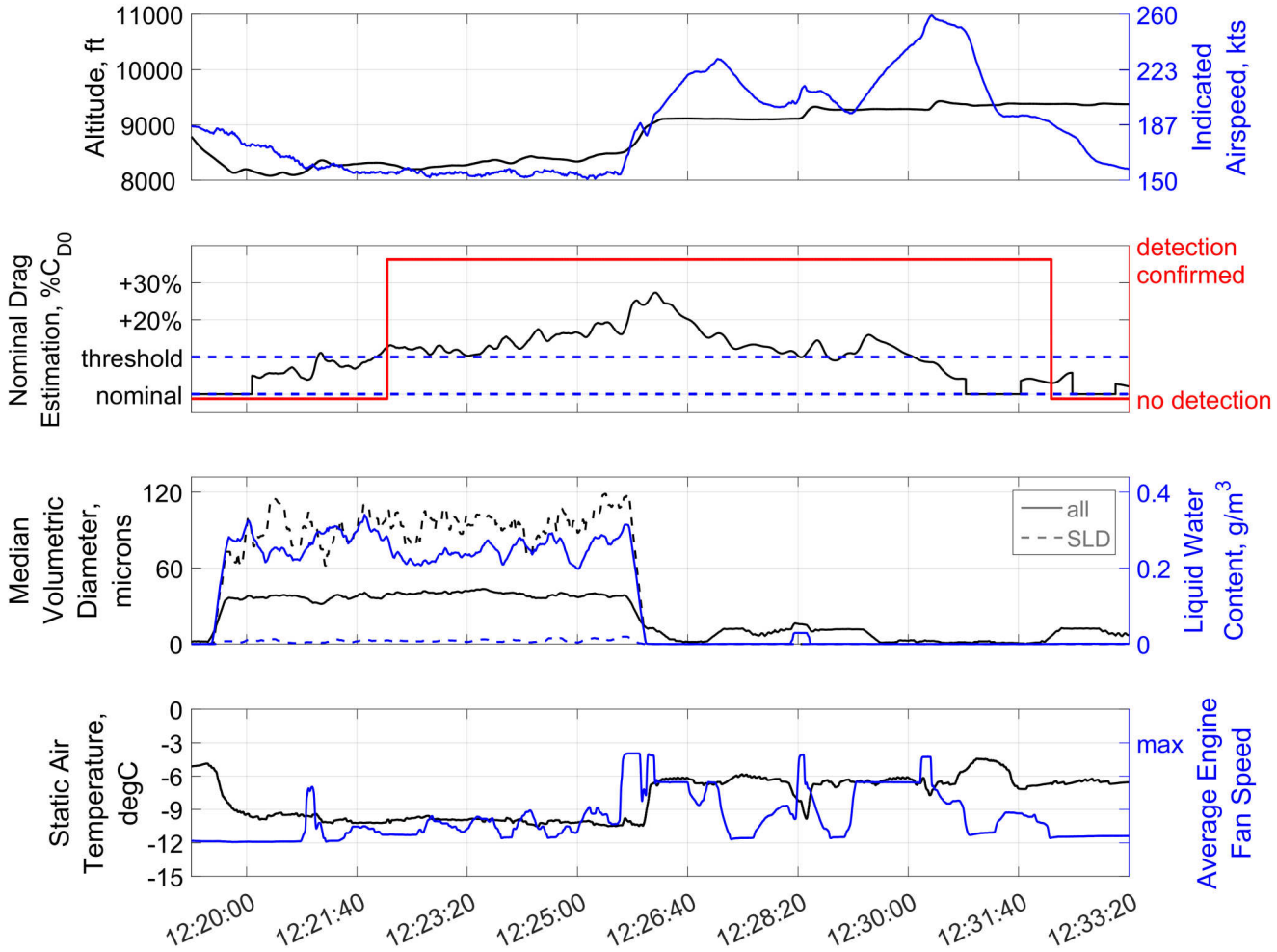

Fig. 11 Time history of IID system performance during specific icing encounter from the example flight (12:19:09 UTC to 12:33:20 UTC): altitude and indicated airspeed (top), relative drag coefficient and IID detection output (second plot), and MVD and LWC of encountered icing conditions including SLD portion (dashed lines) (third plot), and static air temperature and average engine fan speed (bottom); detection threshold at 10 % relative drag increase and adjusted engine thrust model behavior.

The second encounter of this example flight is shown in further detail in Fig. 12 (12:34 UTC to 12:44 UTC). Similar to the first encounter, the aircraft descended into the cloud layer for searching the SLD icing conditions, which started around 12:34:09 UTC resulting again in light ice accretion on unprotected surfaces[2]. After spoiler retractions, the IID outputs the drag estimation which directly shows a drag continuous increase exceeding the detection threshold at around 12:35 UTC approximately one minute after the encounter started. Around four minutes later at 12:38:40 UTC full thrust was applied again to climb out of the icing conditions. It took again around five minutes to restore the nominal flight performance during the subsequent flight with higher speed outside the cloud layer with constant decrease of the estimated drag. At approximately 12:43:10 UTC the IID indication is reset after the detection threshold was undershot around 90 s before. During this encounter the maximum estimated drag increase was around 25% resulting from the moderate ice accretion on the unprotected airframe.

[2]according to Embraer flight test engineer's observation during flight

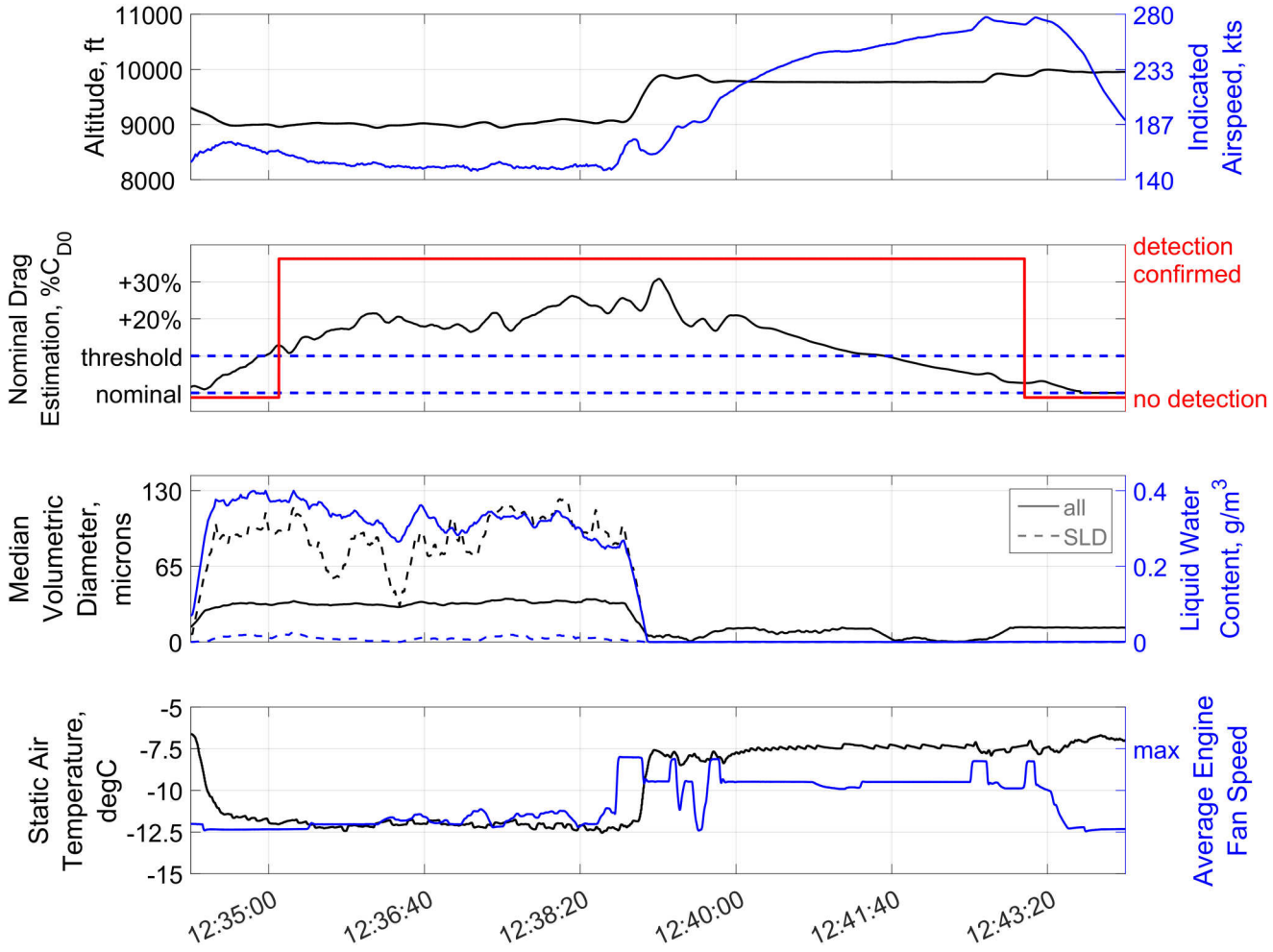

Fig. 12 Time history of IID system performance during specific icing encounter from the example flight (12:34:09 UTC to 12:44:09 UTC): altitude and indicated airspeed (top), relative drag coefficient and IID detection output (second plot), and MVD and LWC of encountered icing conditions including SLD portion (dashed lines) (third plot), and static air temperature and average engine fan speed (bottom); detection threshold at 10 % relative drag increase and adjusted engine thrust model behavior.

The third encounter of this flight in Fig. 13 was conducted in a similar way as the two encounters shown before. Entering SLD icing conditions around 12:46:30 UTC, light ice accumulated on the unprotected surfaces[3]. Estimated drag increases again continuously exceeding the detection threshold around 12:47:20 UTC leading to a positive IID detection. Note that spoiler extension during the descent led to a flatline after 12:46:40 UTC not affecting the detection behavior significantly. After the cloud layer was left and speed was significantly increased the nominal flight performance was restored leading to a reset of IID detection. Again, until the conditions were left the maximum estimated drag increase is around 25% during steady flight with moderate ice accretion on the unprotected surfaces.

During the fourth encounter presented in Fig. 14 (12:58 UTC to 13:08 UTC) similar IID behavior results from moderate ice accretion on the unprotected surfaces[4]. The last encounter before landing in Toledo Airport also result in the same IID behavior due to moderate ice accretion on the unprotected surfaces from similar SLD conditions (13:10 UTC to 13:21 UTC in Fig. 15). Both times the IID fast and reliably indicated the drag increase which finally reached around 25% for the encountered SLD conditions.

[3]according to Embraer flight test engineer's observation during flight
[4]according to Embraer flight test engineer's observation during flight

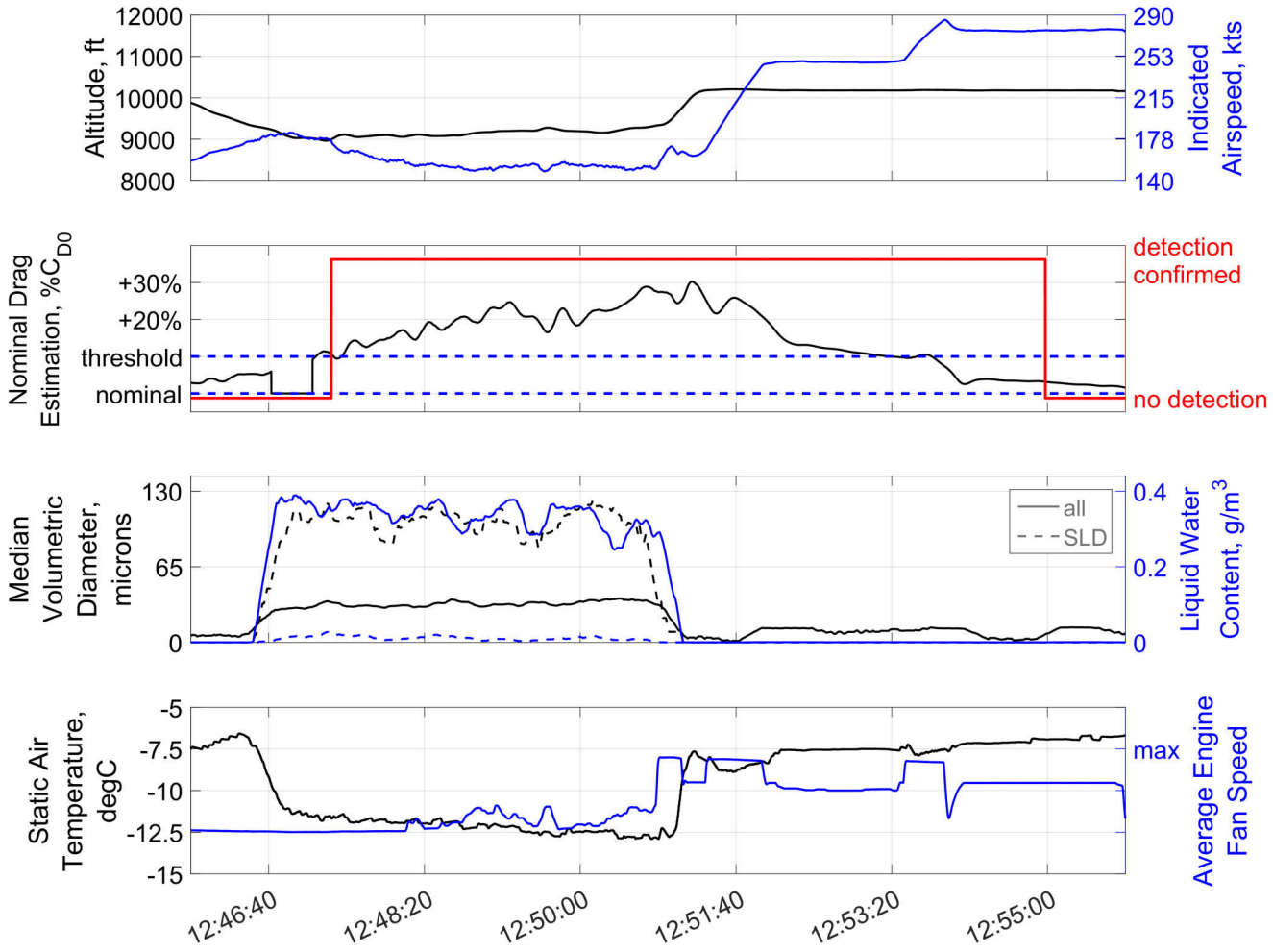

Fig. 13 Time history of IID system performance during specific icing encounter from the example flight (12:45:49 UTC to 12:55:49 UTC): altitude and indicated airspeed (top), relative drag coefficient and IID detection output (second plot), and MVD and LWC of encountered icing conditions including SLD portion (dashed lines) (third plot), and static air temperature and average engine fan speed (bottom); detection threshold at 10 % relative drag increase and adjusted engine thrust model behavior.

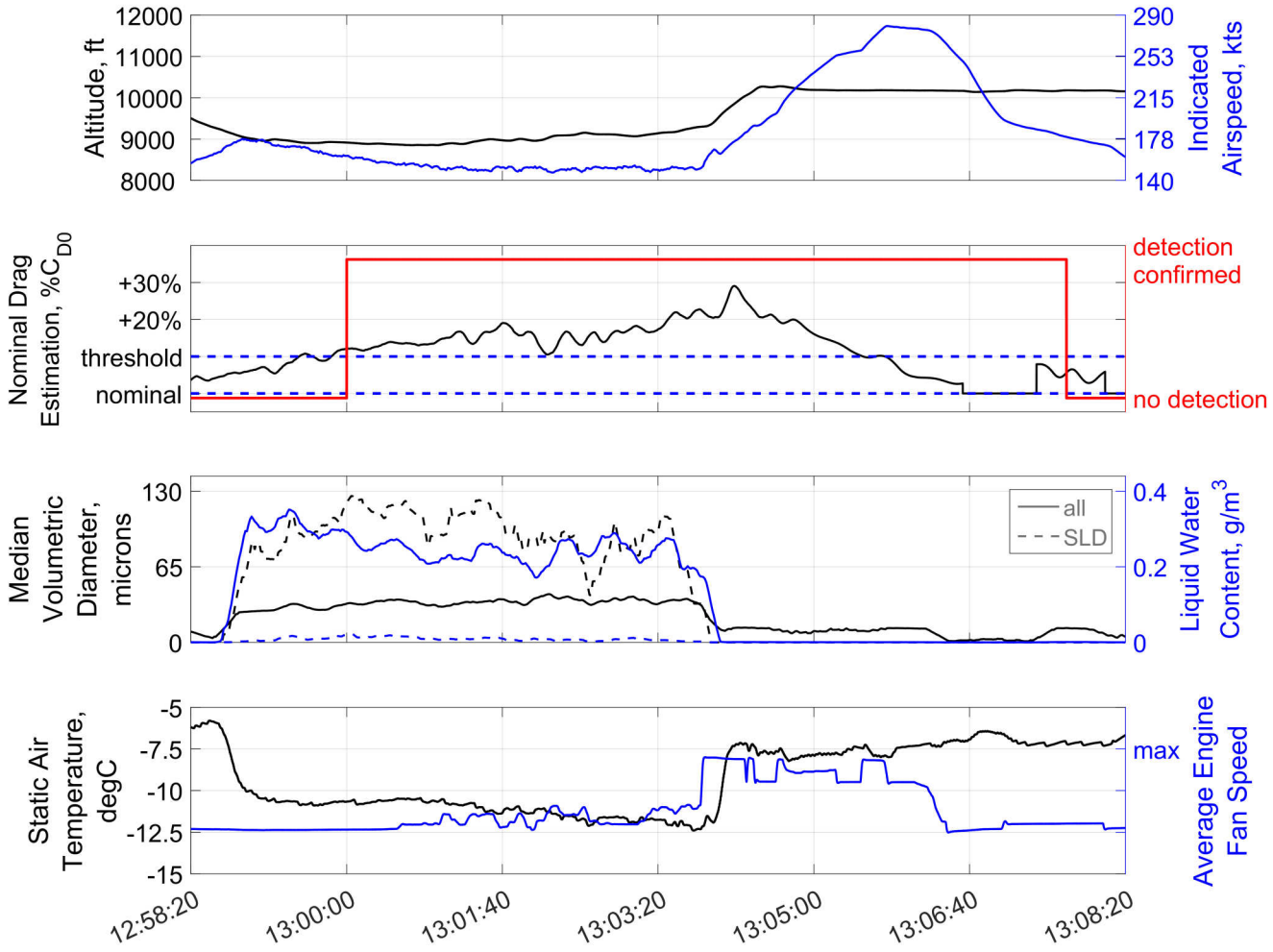

Fig. 14 Time history of IID system performance during specific icing encounter from the example flight (12:58:19 UTC to 13:08:20 UTC): altitude and indicated airspeed (top), relative drag coefficient and IID detection output (second plot), and MVD and LWC of encountered icing conditions including SLD portion (dashed lines) (third plot), and static air temperature and average engine fan speed (bottom); detection threshold at 10 % relative drag increase and adjusted engine thrust model behavior.

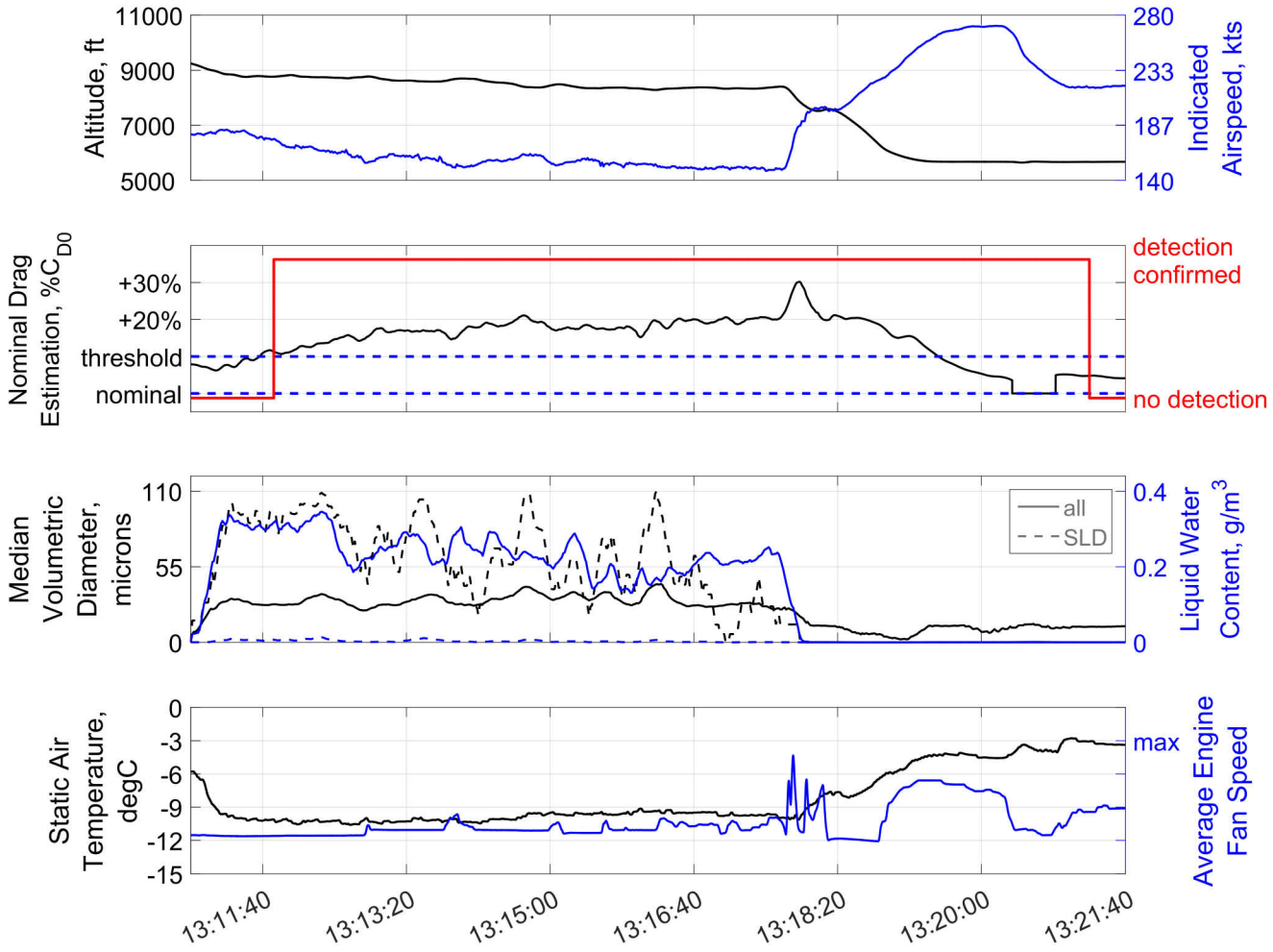

Fig. 15 Time history of IID system performance during specific icing encounter from the example flight (13:10:49 UTC to 13:21:40 UTC): altitude and indicated airspeed (top), relative drag coefficient and IID detection output (second plot), and MVD and LWC of encountered icing conditions including SLD portion (dashed lines) (third plot), and static air temperature and average engine fan speed (bottom); detection threshold at 10 % relative drag increase and adjusted engine thrust model behavior.

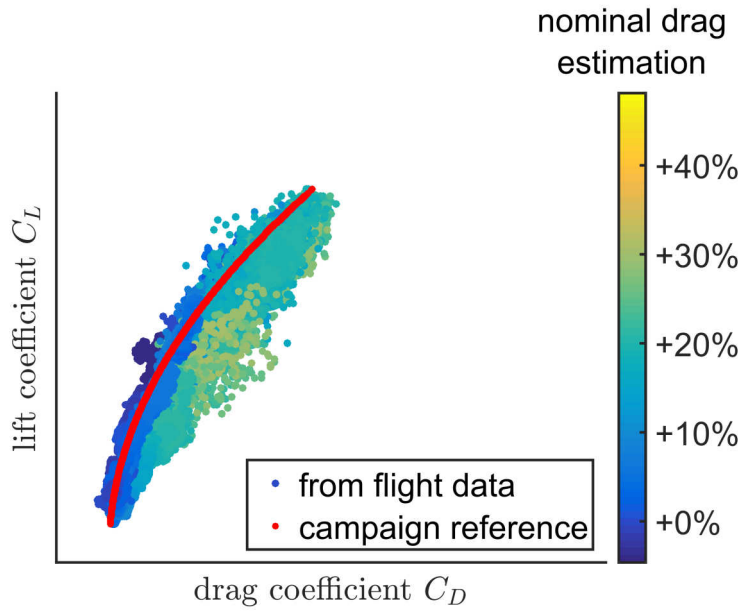

Fig. 16 Aircraft drag polar from example flight (after engine thrust model adjustment): calculated lift and drag coefficient from flight data measurements and reference for the Phenom 300 prototype with SENS4ICE modifications; drag coefficient data including the indication of relative drag calculated by IID with adjusted engine thrust during data replay.

5.1.2 Aerodynamic Degradation due to icing

Figure 16 shows the aircraft drag polar calculated from the measured data for the whole flight (flaps retracted, gear up and no spoiler deflection). For each data point available in the measurement, the lift and drag coefficient is calculated based on the available inertial and inflow measurements as well as the adjusted engine thrust model (see, e.g., Ref. [25] for detailed information on the equations). The plot further contains the aerodynamic reference used for the flight test reflecting the Phenom 300 prototype characteristics with all SENS4ICE modifications (red line). Furthermore, the drag polar data includes an indication of the corresponding IID calculated relative drag (normalized with base aircraft zero-lift drag). Blue marks indicate a nominal drag, which means that there is no increase detected. The more the aircraft is degraded, the more the relative drag increase and the marks are moving to the right getting lighter. Orange marks indicate the maximum calculated drag increase, which has to be taken with caution in the presented case for e.g., the still existing minor shortage of engine thrust approximation used. Anyway, the cyan marks show a drag increase of around 25 % which was approximately the maximum present during the icing encounters as shown in Figs. 11 and 15. Knowing that the main degradation is related to an increase of surface friction on (mainly) unprotected aircraft parts, this is reasonable. This is also well comparable to the results for App. C conditions presented in Ref. [25].

5.1.3 Conclusions on the SLD example flight

With the current available results from the SENS4ICE US flight test campaign and the example flights presented herein and in Ref. [25], the aerodynamic degradation of App. C and SLD (App. O) seem very similar in build-up and magnitude which consequently does not allow to discriminate by the IID alone. Anyway, this was initially anticipated by SENS4ICE and therefore the HIDS concept was developed. The corresponding major result from these flights detailed above and the whole flight test is that the IID is well capable of detecting and announcing any flight performance degradation related to icing until the aircraft is again free of ice again. For the SENS4ICE layered safety approach this means that the IID is able to fulfill the expectations in monitoring the aircraft operational capabilities. Note that this is not a general result for all part of App. C and O, or other aircraft types, or potential

IID implementations. Although the SENS4ICE flight test was very successful in finding SLD icing and having a reasonable icing encounter during the test flight, the conditions are only a very small part of the icing envelope and the ice accretion and hence performance degradation was limited to due flight safety reasons.

5.2 Example from the European flight test campaign

Results from one specific flight of the European icing flight test campaign are presented and evaluated. During this flight different icing conditions including classical App. C and the rare SLD conditions (App. O) were successfully encountered on April 24th, 2023 in Southern France. Note that for safety reasons, the mechanical de-icing system of the ATR42, i.e. pneumatic boots, was activated during the encounters according to the given operational requirements, which led mainly to intercycle ice shapes[5] on the wing's and horizontal tail's leading edges. Figure 17 contains an overview of the flight track from the flight around the CERs Marsan and Cazaux west of Toulouse. The flight track is color-coded with the information retreived from the reference accretion sensor under the left wing of the aircraft for three different states: no ice, ice accretion up to 0.02 in and ice accretion above 0.02 in, without any further information on the specific type or shape of the ice. It can be clearly seen, that during the flight icing was encountered at a specific altitude and after a certain time, the aircraft descended to perform a full airframe de-icing in warmer air.

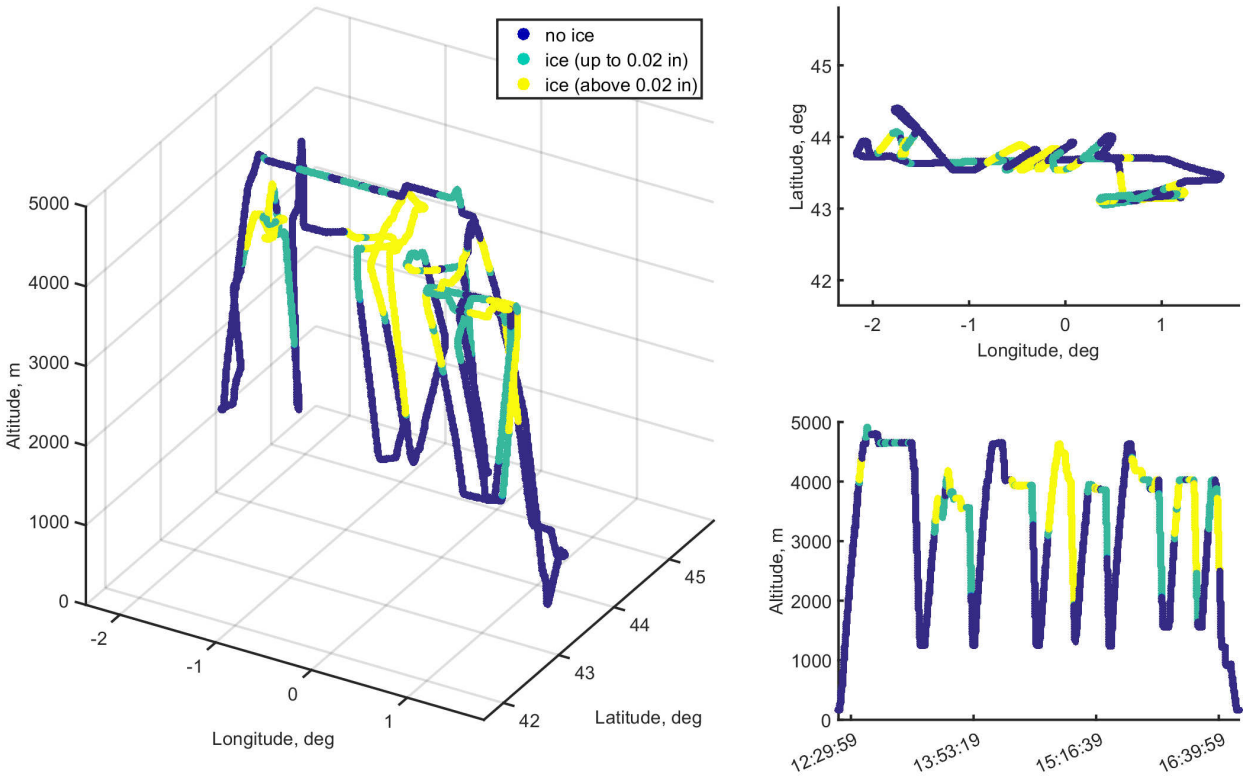

Fig. 17 Flight track from SENS4ICE European icing campaign flight on April 24th, 2023 around Toulouse/Marsan/Cazaux: geodetic position and altitude with indication of icing encountered / build-up.

[5]ice shapes forming between the cyclic activation of the mechanical de-icing system, i.e., pneumatic boots

5.2.1 Indirect ice detection system performance during European campaign flight

A time history of the IID detection behavior during this specific flight is given in Fig. 18. The four different plots contain: altitude and indicated airspeed (top), nominal drag estimation and IID detection output (second plot), ice build-up on aircraft ice accretion sensor and static air temperature (third plot), and MVD and LWC of encountered icing conditions (solid line) including the indication of the amount of SLD (dashed lines) (bottom). During the flight testing a threshold for the detection of 15 % drag increase compared to the nominal flight performance was set. It could be seen, that the major icing events / encounter also led to a confirmed detection of abnormal flight performance through the IID. But after the campaign it was found that a modified and reduced threshold of 10 % could significantly enhance the IID performance and reactivity without any negative effect, e.g., false alarms. In addition, the intercycle ice (partly removed ice accretion from the leading at after activation of the de-icing boots) led sometimes to a reduction of drag increase below the detection threshold (e.g., Fig. 18 around 12:55 UTC or around 13:05 UTC) resetting the IID detection although the flight performance is still degraded and the encounter continuous. This switching behavior is physically correct, but undesired. It could be overcome with further output filtering or enhanced output logic, but a more reliable IID behavior with even lower thresholds is even more favorable.

Figure 19 shows the same flight as a result from an IID post flight replay with a reduced threshold of 10 % drag increase. Again, there is no significant difference between both results except for the detection output. The IID output now indicates the icing encounters in a continuous manner, without any switches between the detection state. Hence, the results presented in the following will contain the reduced detection threshold (10 %) instead of the more conservative flight test threshold (15 %).

Figures 20 and 21 show the first two encounters (between 12:30:00 UTC and 13:16:55 UTC, and 13:24:40 UTC to 13:53:20 UTC) in more detail: in both cases the performance degradation is very slow in the beginning and the detection threshold (10 %) is exceeded after around 10 min. The first encounter does not cause any significant aerodynamic impact in the beginning, which consequently is not visible in the IID output. Anyway, as long as icing conditions do not significantly alter the aircraft characteristics, there is no potential safety issue for the further flight operations present. The moment the drag increases due to more significant ice accretion on the airframe, the IID correctly and reliably indicates an abnormal flight performance (around 12:48 UTC). Similarly, during the second encounter, the degradation in the beginning is very small and does not exceed the threshold while nearly reaching it around 13:31 UTC. The degradation was reduced again before rising significantly, presumably due to a combination of the de-icing system and (static air) temperatures near 0 degC. Nevertheless, at around 13:34 UTC, significant icing conditions were encountered leading to an ice formation on the airframe again (indicated by the icing probe signal) which caused a fast and detectable performance degradation with respect to aircraft drag increase (up to 25 % above the nominal value of the drag estimation). Hence, the IID directly indicates the abnormal performance after exceeding the detection threshold (around 13:35 UTC).

Figure 22 shows the third encounter of this flight, which had a different profile than the previous ones. This time, the icing conditions directly led to a significant ice formation on the airframe (indicated through the jump in the aircraft ice accretion sensor signal) which is directly correlated with the strong icing situation also related to SLD. The aircraft performance is continuously degraded until it reaches more than 50 % relative drag increase compared to the nominal value. This degradation persists although the icing situation changes to even larger drops (see bottom plot at around 14:29 UTC). Due to the fact, that the de-icing boots were activated during the encounter, the aircraft was protected and a further aerodynamic degradation was prevented. The IID confirmed the ice formation on the airframe through the monitoring of the aircraft's flight performance within less than a minute after the encounters started. For this encounter pictures from the cameras indicting the airframe icing situation are available. Figure 23 shows a specific view on the leading edges of left and right wing (from below) together with the horizontal tail for different times. At 14:19:25 UTC when the encounter started, the airframe was free of visible ice

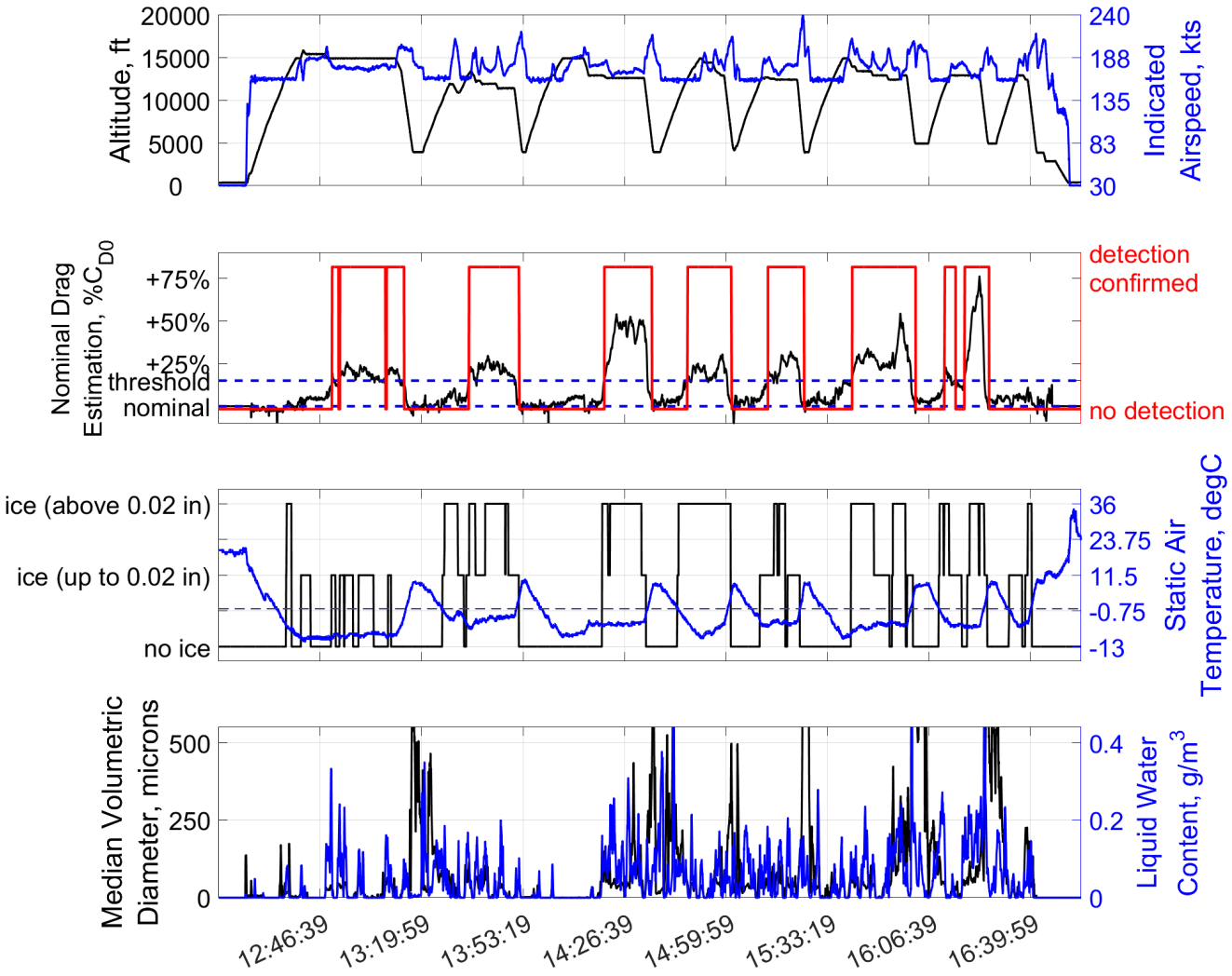

Fig. 18 Time history of IID system performance during the example flight on April 24th, 2023 (12:13 UTC to 16:56 UTC): altitude and indicated airspeed (top), nominal drag estimation and IID detection output (second plot), ice build-up on aircraft ice accretion sensor and static air temperature (dashed line 0 degC) (third plot), and MVD and LWC of encountered icing conditions (solid line) including the indication of the amount of SLD (dashed lines) (bottom), vertical zoom limiting plot to icing conditions neglecting rain above freezing point; original detection threshold at 15 % relative drag increase.

accretion. But around two minutes later and a confirmed IID detection information, the airframe shows an icing layer which is already broken on the wing leading edges by the active de-icing system. During the next minutes the formation does not change in total and although the boots allow to remove some ice, new formations build up, which then cause almost no change in the estimated drag resulting from the IID. It is interesting to see that at around 14:29 UTC, when large drops were encountered, the wings seem to have less ice accretion than before – resulting in the reduction of the additional drag estimated by the IID between 14:29 UTC and 14:31 UTC – because of a presumably good effectivity of the protection system. The drag rises again briefly after, where a more glaze ice looking ice formation is visible on the aircraft (14:32:37 UTC in Fig. 23), which is presumably a result of the ongoing SLD icing situation. Anyway, this result shows that a currently present encounter might not have instantaneously a noticeable adverse effect on the aircraft aerodynamics. Monitoring only the icing conditions might consequently not give a correct indication on the criticality of the encounter even if the situation looks dangerous in terms of water drops in the air. But the continuous monitoring of the ice formation and corresponding aerodynamics degradation will give the comprehensive view on the current situation required for a safe

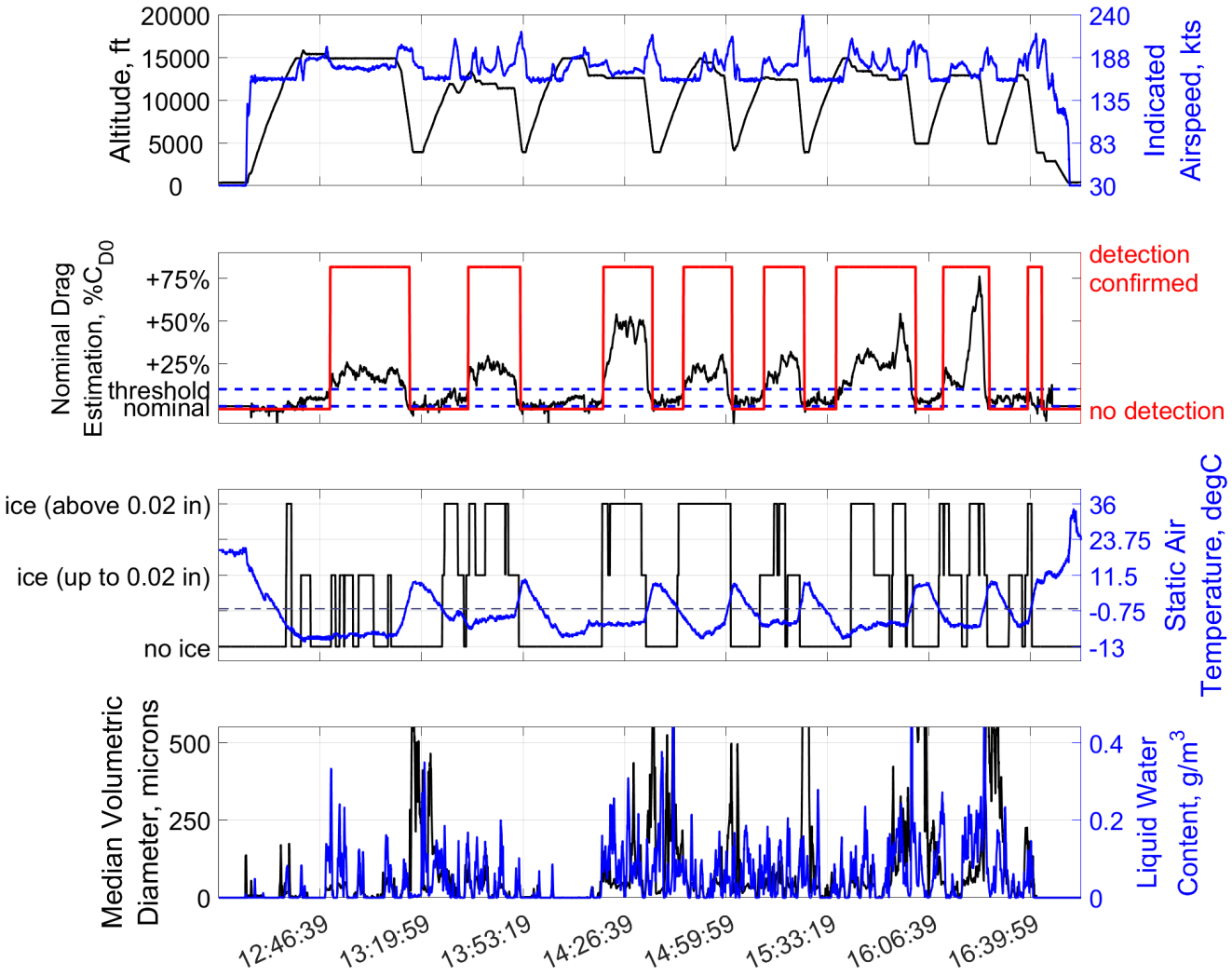

Fig. 19 Time history of IID system performance during the example flight on April 24th, 2023 (12:13 UTC to 16:56 UTC): altitude and indicated airspeed (top), nominal drag estimation and IID detection output (second plot), ice build-up on aircraft ice accretion sensor and static air temperature (dashed line 0 degC) (third plot), and MVD and LWC of encountered icing conditions (solid line) including the indication of the amount of SLD (dashed lines) (bottom), vertical zoom limiting plot to icing conditions neglecting rain above freezing point; updated detection threshold at 10 % relative drag increase.

aircraft operation. After descending and passing through the 0 degC temperature layer, the aircraft got free of ice again (14:36 UTC).

Similar results can be obtained for the next encounter between 14:42:29 UTC and 15:02:39 UTC given in Fig. 24 (time history plot) and Fig. 25 (camera footage). During the climb to flight level 140 the aircraft entered icing conditions leading to an airframe ice accretion indicated by the aircraft ice accretion sensor. At around 14:46 UTC, the aircraft's wings and empennage are visibly free of ice, which means that ice formation was presumably only present on the unprotected surfaces resulting in less than 10 % relative drag deviation. But, during the following climb the aircraft performance was notably degraded and the IID correctly announced the performance loss. At 14:49:15 UTC the wings' leading edges had some ice formation corresponding to approximately 25 % increase in the nominal drag estimation. The situation was maintained almost unchanged in terms of ice formation and degradation until the aircraft descended after 15:00 UTC into warmer air to remove the ice completely. Note that this encounter

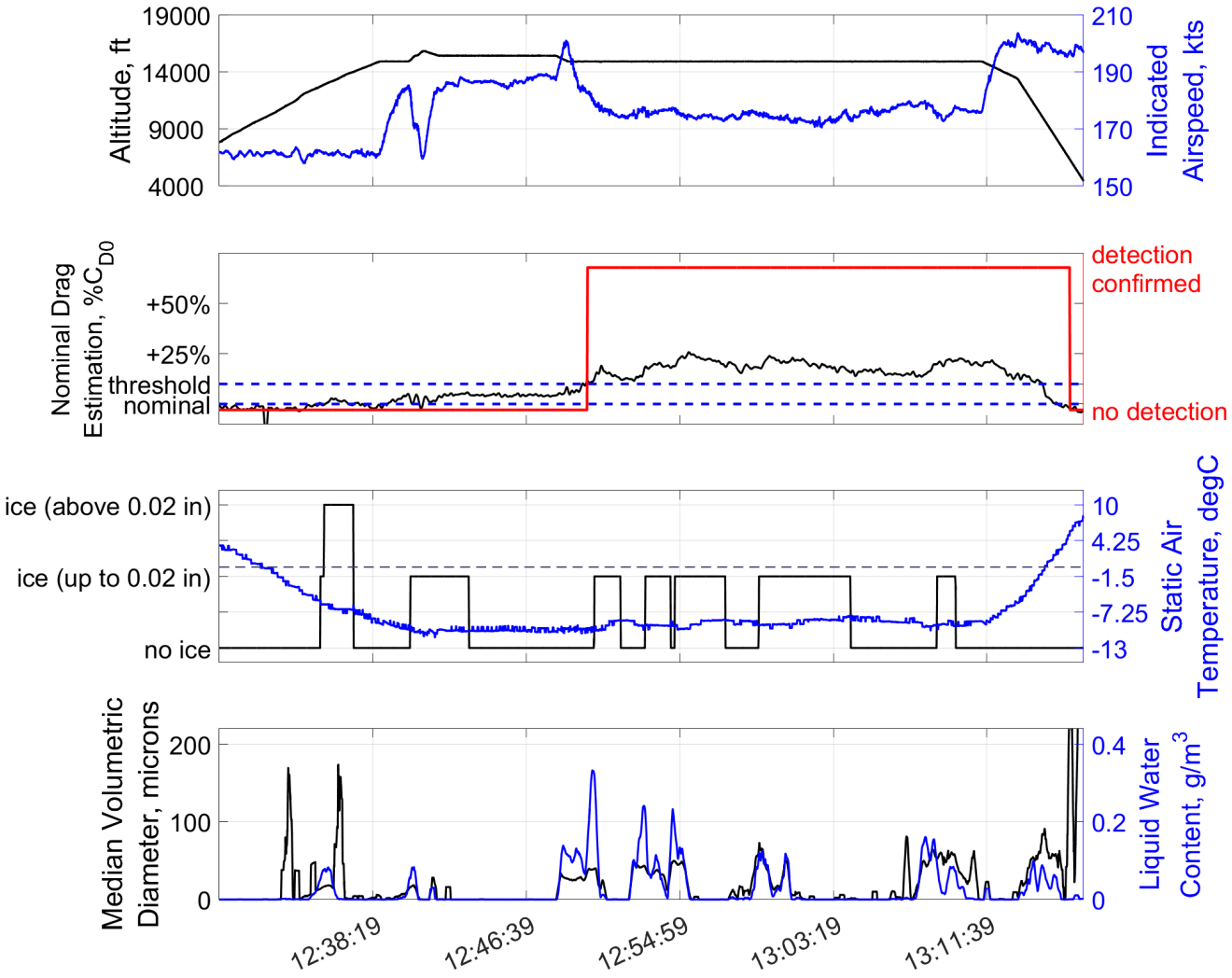

Fig. 20 Time history of IID system performance during specific encounter of the example flight on April 24th, 2023 (12:30:00 UTC to 13:16:55 UTC): altitude and indicated airspeed (top), nominal drag estimation and IID detection output (second plot), ice build-up on aircraft ice accretion sensor and static air temperature (dashed line 0 degC) (third plot), and MVD and LWC of encountered icing conditions (solid line) including the indication of the amount of SLD (dashed lines) (bottom), vertical zoom limiting plot to icing conditions neglecting rain above freezing point; updated detection threshold at 10 % relative drag increase.

shows the advantage of the IID working throughout all flight conditions resulting in a fast and reliable information on the icing related performance degradation.

The next encounter in Figs. 26 and 27 was quite similar in terms of aerodynamic degradation characteristics and IID results. The aircraft climbed above FL120 and encountered icing condition leading more or less directly to an indication of ice accretion on the aircraft ice accretion sensor. At 15:12:10 UTC the aircraft shows no ice accretion on the wing or empennage, but less than one minute later the IID provides an abnormal performance detection when the nominal drag estimation exceeds the 10 % threshold. At 15:13:50 UTC light ice formation is clearly visible on the airframe. Again, the IID is able to fast and reliably indicate the aerodynamic degradation pointing to an ice contamination on the airframe. Throughout the encounter the degradation was increasing when the ice formation on the airframe rises (e.g., at 15:19:08 UTC). After the aircraft entered warmer air, the ice was removed and the nominal flight performance restored.

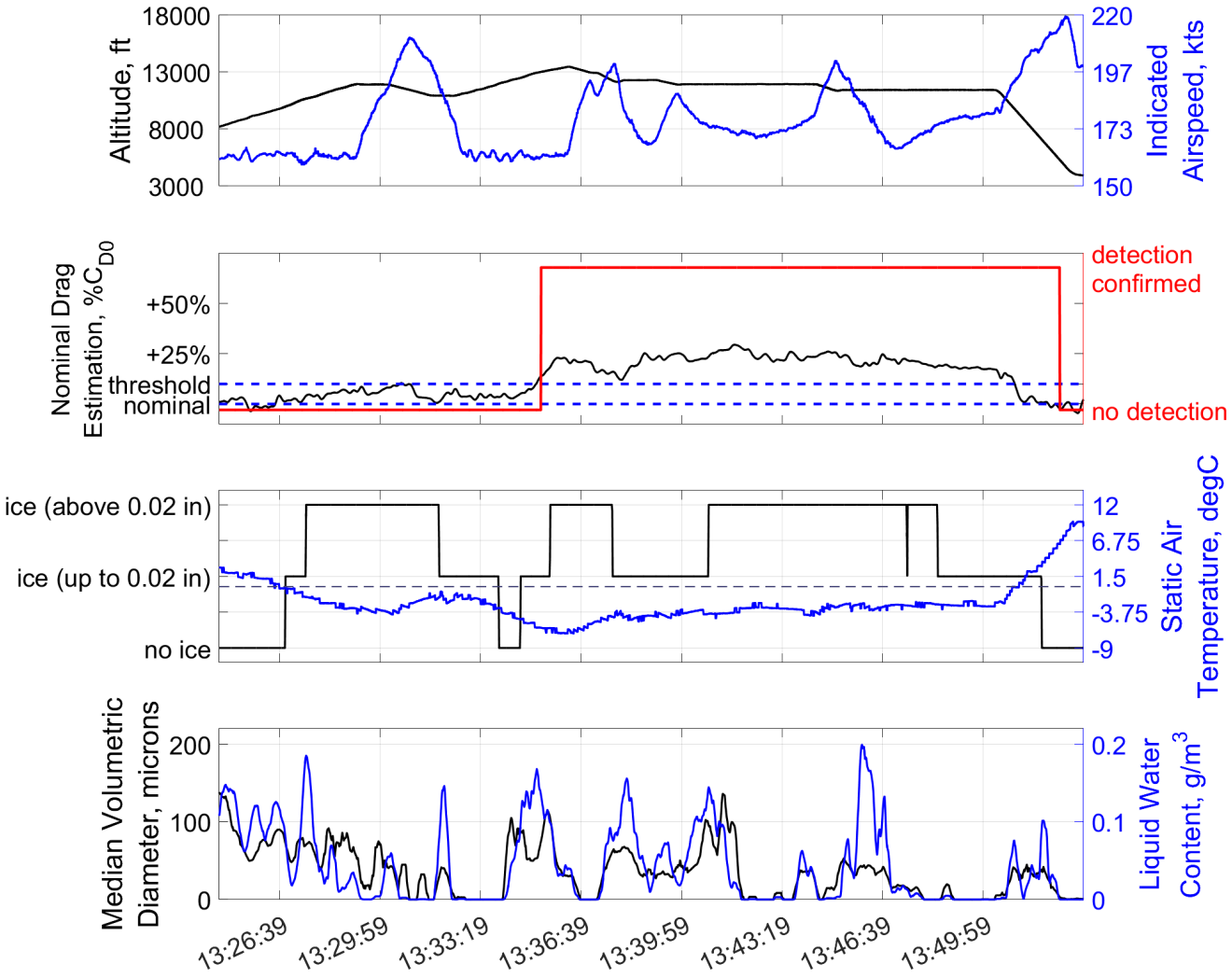

Fig. 21 Time history of IID system performance during specific encounter of the example flight on April 24th, 2023 (13:24:40 UTC to 13:53:20 UTC): altitude and indicated airspeed (top), nominal drag estimation and IID detection output (second plot), ice build-up on aircraft ice accretion sensor and static air temperature (dashed line 0 degC) (third plot), and MVD and LWC of encountered icing conditions (solid line) including the indication of the amount of SLD (dashed lines) (bottom), vertical zoom limiting plot to icing conditions neglecting rain above freezing point; updated detection threshold at 10 % relative drag increase.

The sixth encounter of this flight (Figs. 28 and 29) also shows a very interesting aerodynamic degradation characteristic underlining the benefits of the IID for a comprehensive picture of the aircraft icing situation and for maintaining a safe flight condition during all-weather operations. Icing conditions are again encountered during the climb into the cloud layer and the drag estimation indicates relatively fast a degradation compared to the nominal case for the flight test. Before level off, the IID confirms an abnormal flight performance and maintains this warning throughout the whole encounter. Ice accretion is visible on the airframe at 15:38 UTC whereas the aircraft ice accretion sensor gives no indication. Also, the reference sensors do not show any icing conditions at around 15:39 UTC but the aircraft is still iced and drag increased (10 % to 15 %). After 15:40 UTC the aircraft ice accretion sensor and the atmospheric reference sensors indicate icing conditions with significant accretion and the aerodynamics are further degraded (more than 25 % relative increase compared to nominal values). Between 15:49 UTC and 15:54 UTC the aircraft ice accretion sensor reduced the indication to small accretion and no ice and the conditions were characterized by small numbers of droplets but the aircraft was still degraded, correctly indicated by the IID. After 15:54 UTC SLDs are encountered again and a significant ice accretion on the

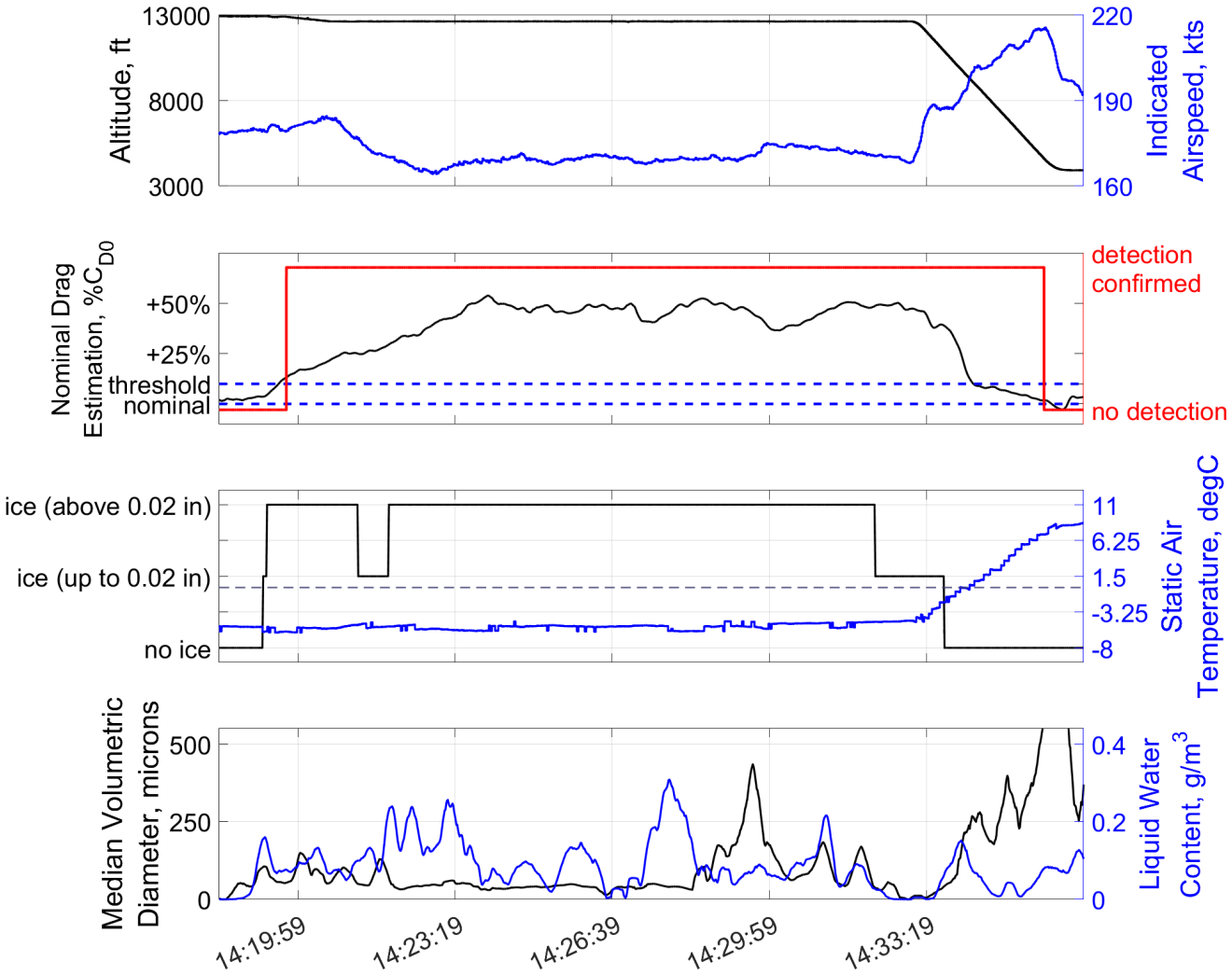

Fig. 22 Time history of IID system performance during specific encounter of the example flight on April 24th, 2023 (14:18:20 UTC to 14:36:40 UTC): altitude and indicated airspeed (top), nominal drag estimation and IID detection output (second plot), ice build-up on aircraft ice accretion sensor and static air temperature (dashed line 0 degC) (third plot), and MVD and LWC of encountered icing conditions (solid line) including the indication of the amount of SLD (dashed lines) (bottom), vertical zoom limiting plot to icing conditions neglecting rain above freezing point; updated detection threshold at 10 % relative drag increase.

airframe is visible which leads to a relative drag increase (constant rise during encounter to maximum value) of about 50 % above nominal. Descending to warmer air quickly removed the ice afterwards restoring the aircraft's nominal flight performance.

During the last encounter of this flight in Figs. 30 and 31 the maximum performance degradation was observed. Climbing into the icing conditions directly caused a positive ice indication from the aircraft ice accretion sensor when passing 0 degC with supercooled liquid water present in the air. Around 16:11:20 UTC the IID also confirmed a performance degradation with estimated drag increasing above the 10 % threshold in climb phase. Reaching the target altitude fewer icing conditions were found but the aircraft ice accretion sensor (ice above 0.02 in) and IID still indicate icing, showing again, that the degradation is still present although icing conditions have already been left. Figure 31 indicates that only light ice formation was visible on the airframe during this period. A new cloud with icing conditions was entered around 16:17 UTC and icing is still announced by the IID due to the still existing drag increase, but at 16:17:30 UTC the aircraft ice accretion sensor was reset to clean, while the estimated drag was

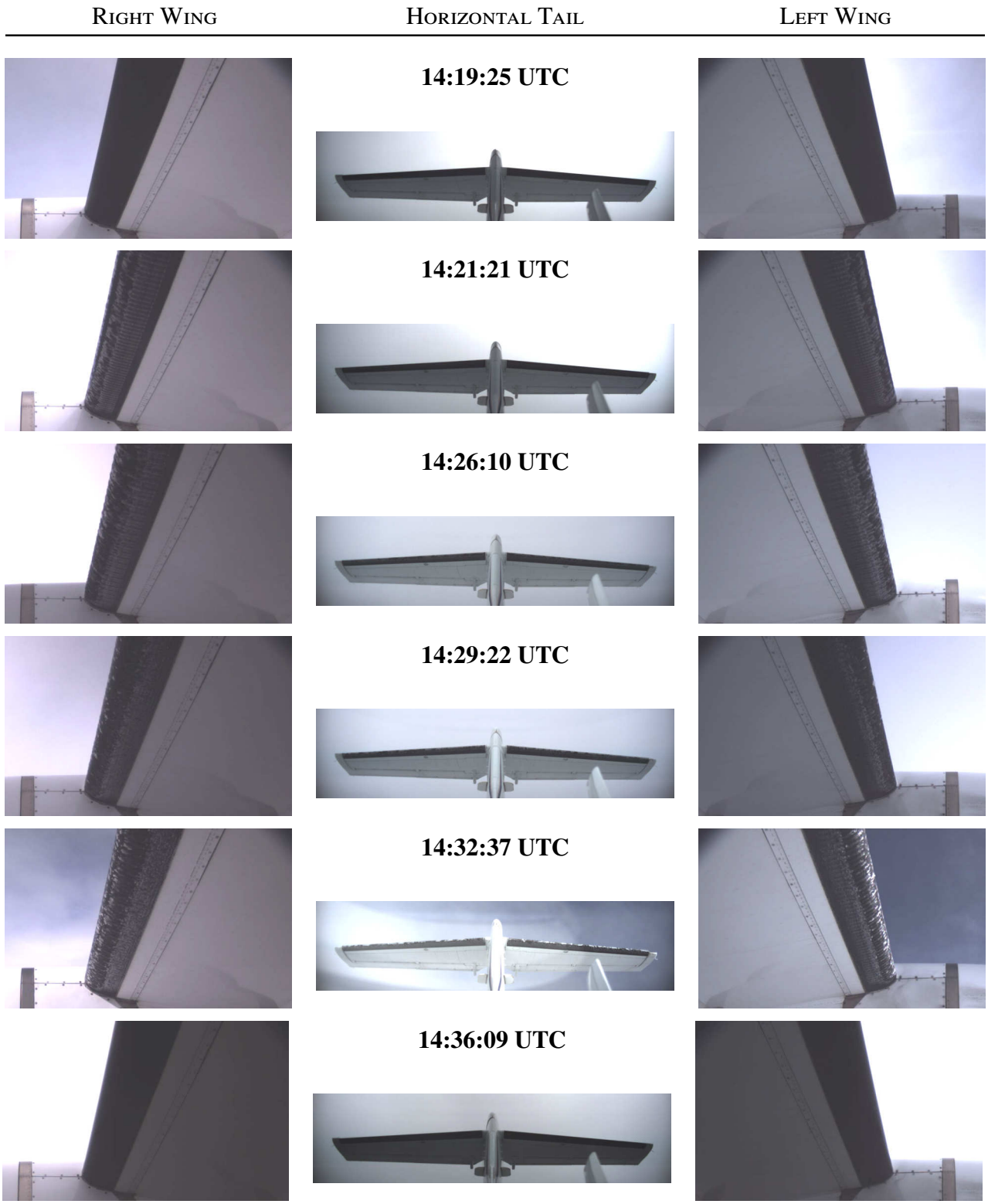

Fig. 23 Evolution of ice accretion on the airframe during icing encounter: camera views on left & right wing and horizontal tail for specific moments during flight (increased brightness and contrast); corresponding to encounter and IID detection given in Fig. 22; credit Safire / SENS4ICE project.

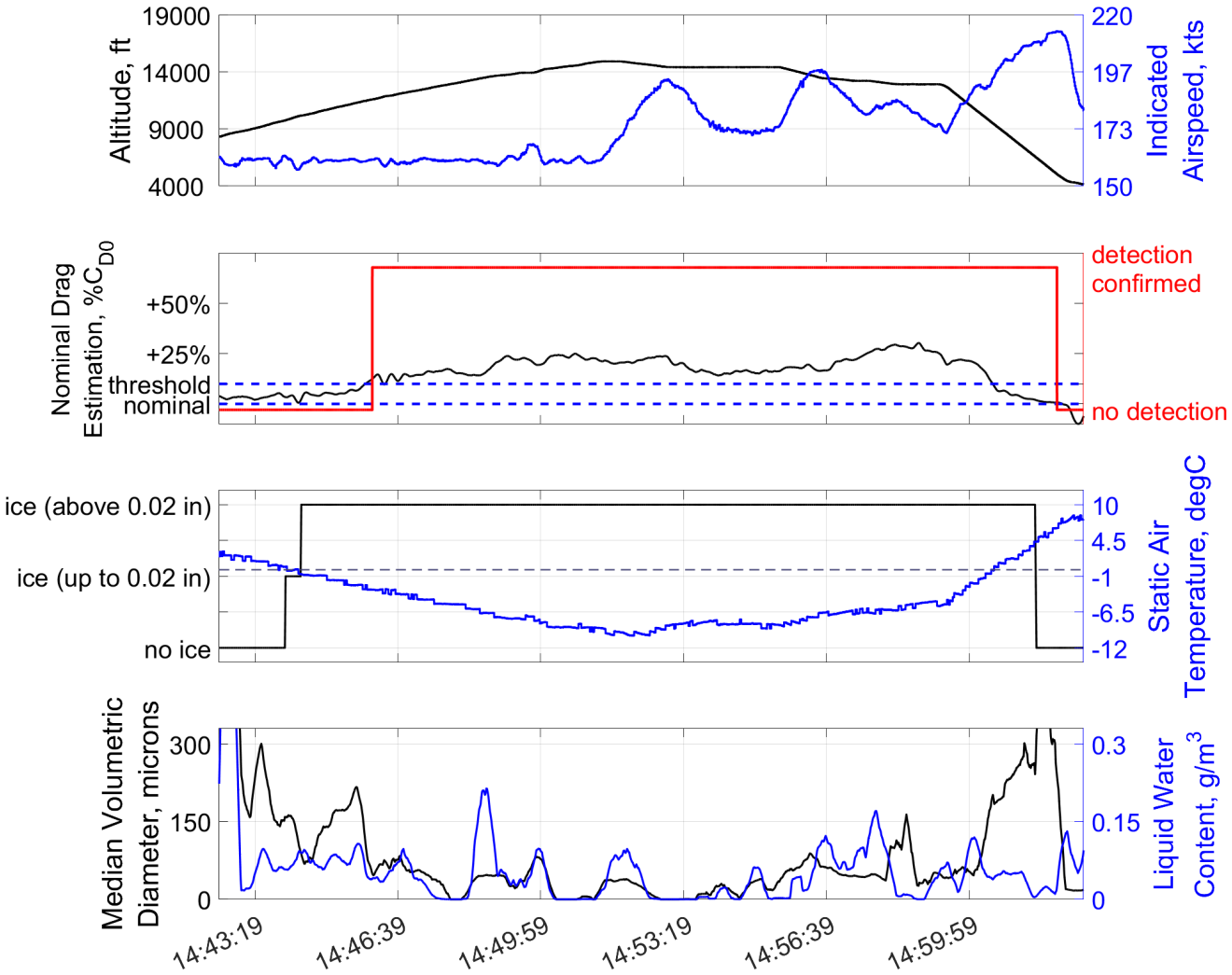

Fig. 24 Time history of IID system performance during specific encounter of the example flight on April 24th, 2023 (14:42:30 UTC to 15:02:40 UTC): altitude and indicated airspeed (top), nominal drag estimation and IID detection output (second plot), ice build-up on aircraft ice accretion sensor and static air temperature (dashed line 0 degC) (third plot), and MVD and LWC of encountered icing conditions (solid line) including the indication of the amount of SLD (dashed lines) (bottom), vertical zoom limiting plot to icing conditions neglecting rain above freezing point; updated detection threshold at 10 % relative drag increase.

increasing significantly. After 16:19 UTC IID, the aircraft ice accretion sensor and the measurements of atmospheric conditions clearly indicate icing conditions, also containing larger droplets with higher water content. The maximum estimated drag increase was above 75 % at 16:23:10 UTC well matching the significant ice formation shown in Fig. 31 at the corresponding time. This encounter also shows the need for a comprehensive view on the aircraft icing situations and the monitoring of the aircraft capabilities to be not misled by individual indications. After descending into warmer air and leaving the icing conditions, the aircraft's nominal performance was restored and the IID detection output reset.

Note again, that during all encounters the de-icing system of the Safire ATR 42 was active and ice was shed from protected areas during the whole flight. Otherwise, the performance degradation might have been significantly higher with a potential threat to a safe flight operation. Hence, for some conditions the aerodynamic degradation maintains relatively constant because the overall accretion was kept on a manageable level.

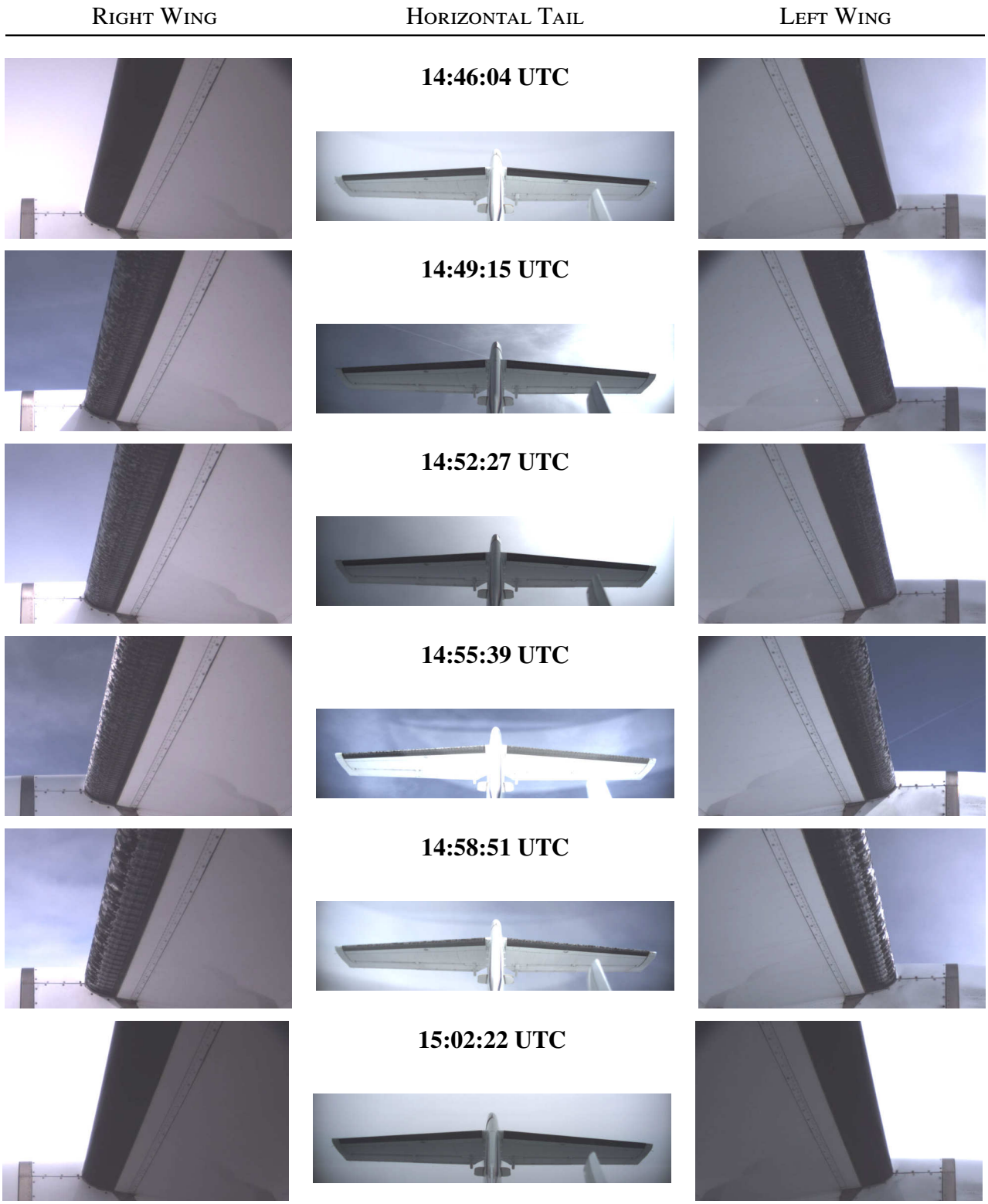

Fig. 25 Evolution of ice accretion on the airframe during icing encounter: camera views on left & right wing and horizontal tail for specific moments during flight (increased brightness and contrast); corresponding to encounter and IID detection given in Fig. 24; credit Safire / SENS4ICE project.

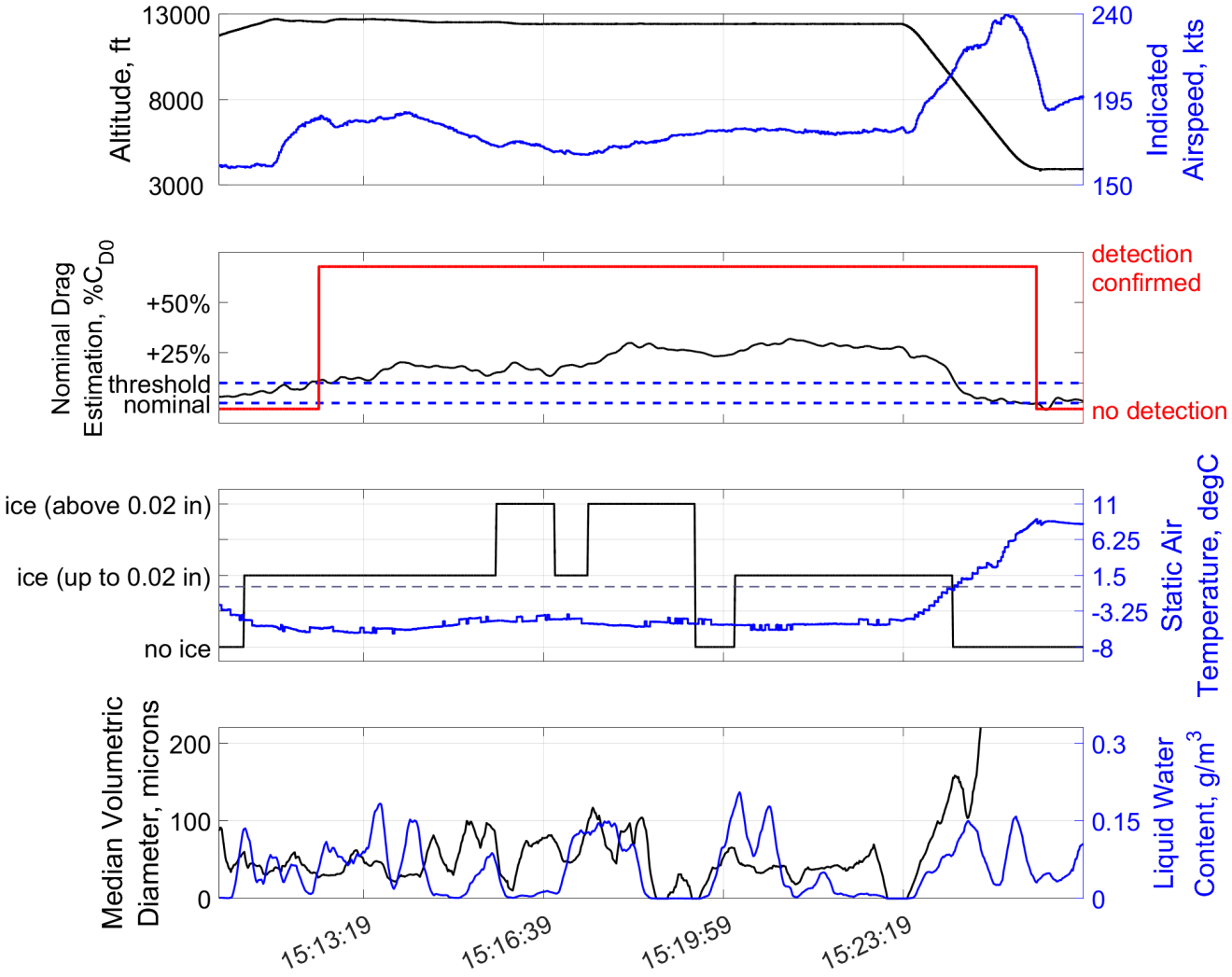

Fig. 26 Time history of IID system performance during specific encounter of the example flight on April 24th, 2023 (15:10:40 UTC to 15:26:40 UTC): altitude and indicated airspeed (top), nominal drag estimation and IID detection output (second plot), ice build-up on aircraft ice accretion sensor and static air temperature (dashed line 0 degC) (third plot), and MVD and LWC of encountered icing conditions (solid line) including the indication of the amount of SLD (dashed lines) (bottom), vertical zoom limiting plot to icing conditions neglecting rain above freezing point; updated detection threshold at 10 % relative drag increase.

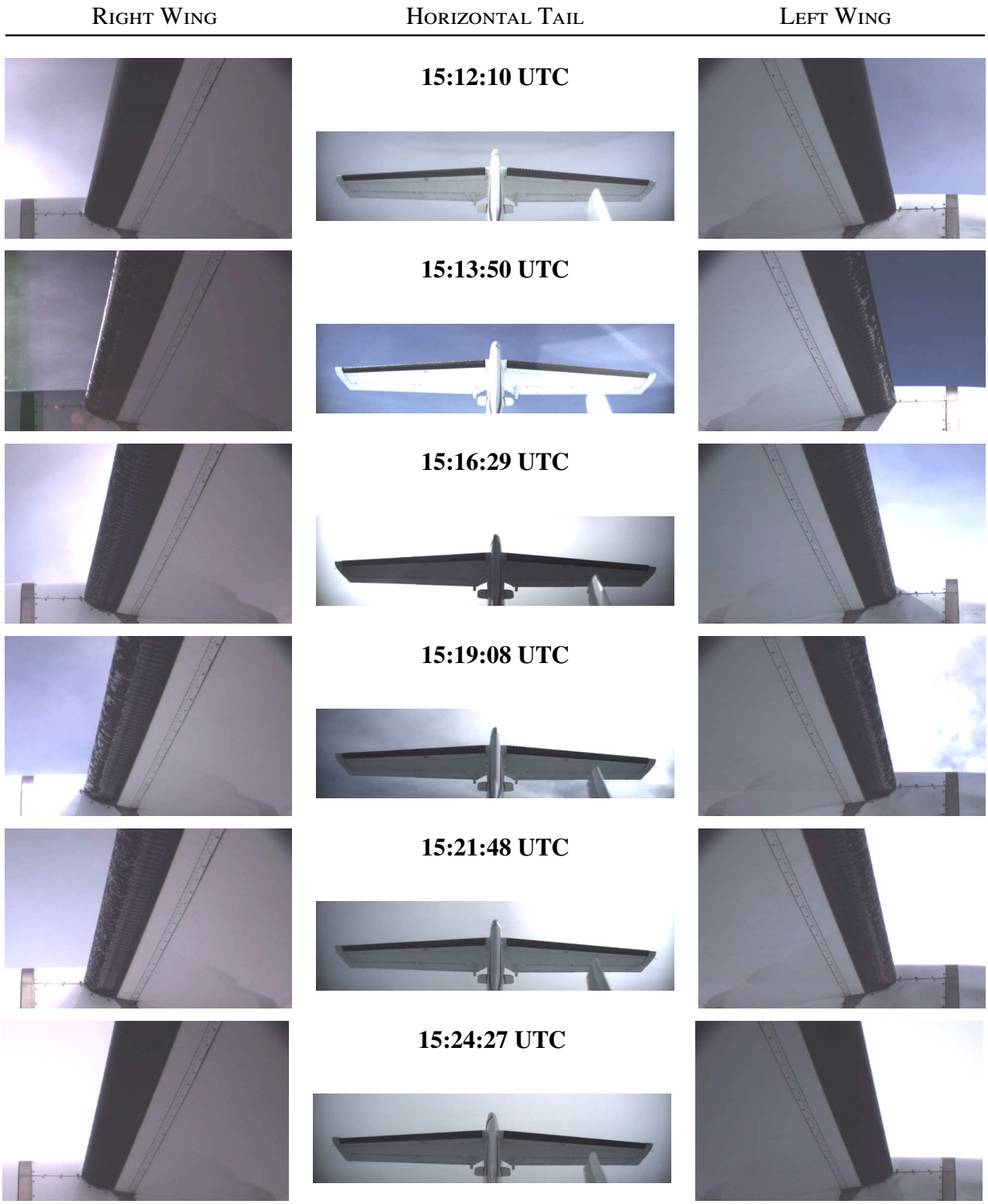

Fig. 27 Evolution of ice accretion on the airframe during icing encounter: camera views on left & right wing and horizontal tail for specific moments during flight (increased brightness and contrast); corresponding to encounter and IID detection given in Fig. 26; credit Safire / SENS4ICE project.

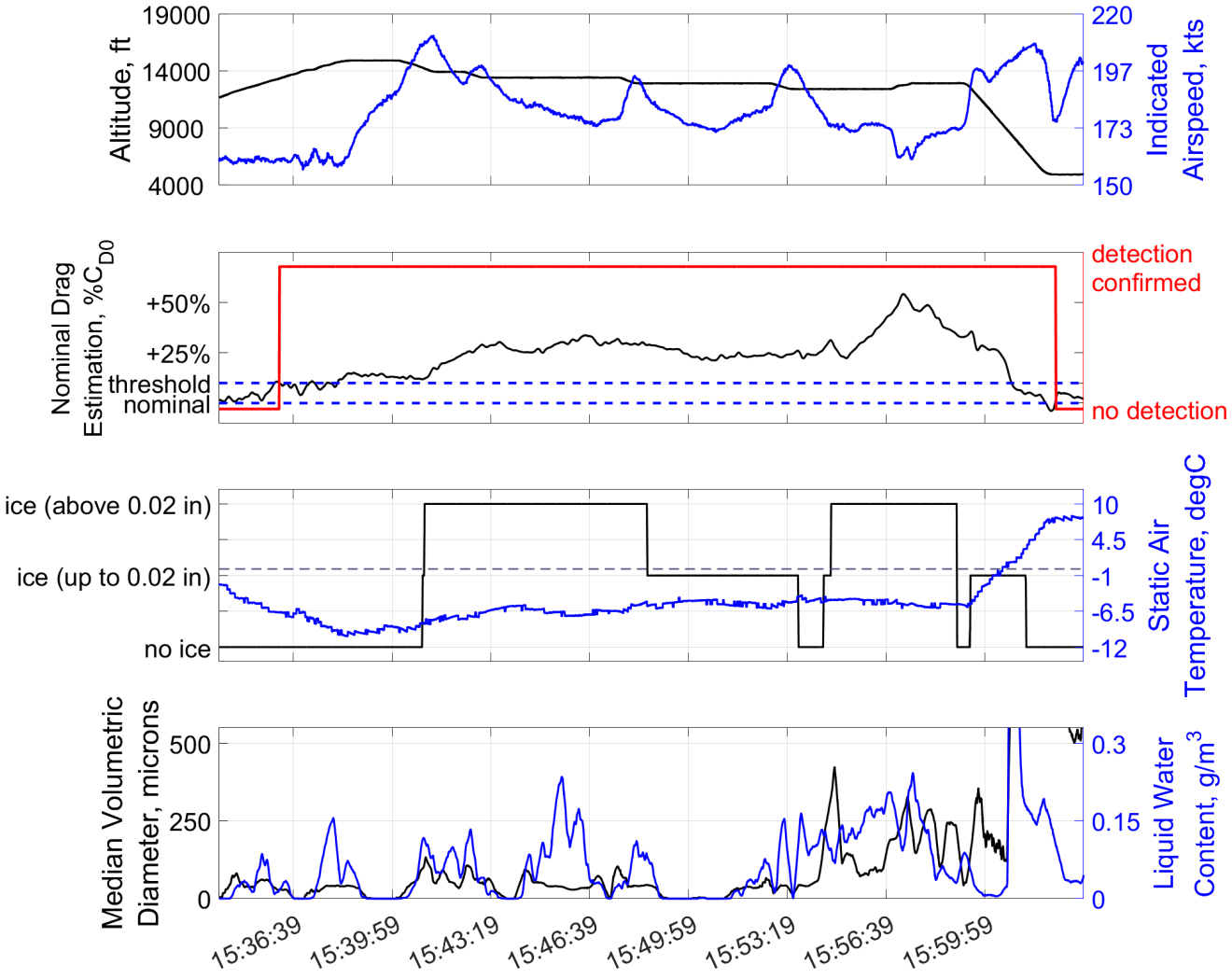

Fig. 28 Time history of IID system performance during specific encounter of the example flight on April 24th, 2023 (15:34:09 UTC to 16:03:19 UTC): altitude and indicated airspeed (top), nominal drag estimation and IID detection output (second plot), ice build-up on aircraft ice accretion sensor and static air temperature (dashed line 0 degC) (third plot), and MVD and LWC of encountered icing conditions (solid line) including the indication of the amount of SLD (dashed lines) (bottom), vertical zoom limiting plot to icing conditions neglecting rain above freezing point; updated detection threshold at 10 % relative drag increase.

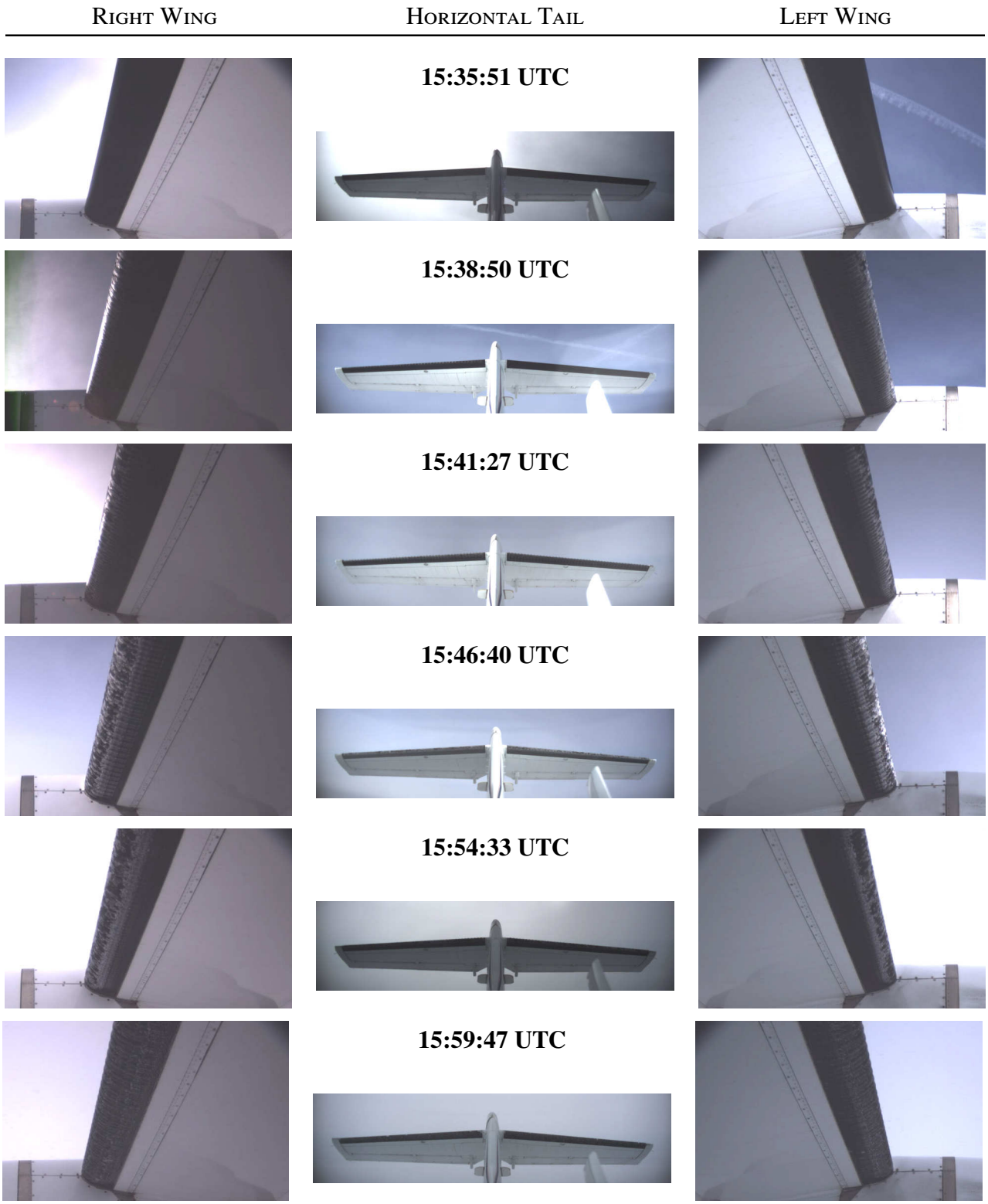

Fig. 29 Evolution of ice accretion on the airframe during icing encounter: camera views on left & right wing and horizontal tail for specific moments during flight (increased brightness and contrast); corresponding to encounter and IID detection given in Fig. 28; credit Safire / SENS4ICE project.

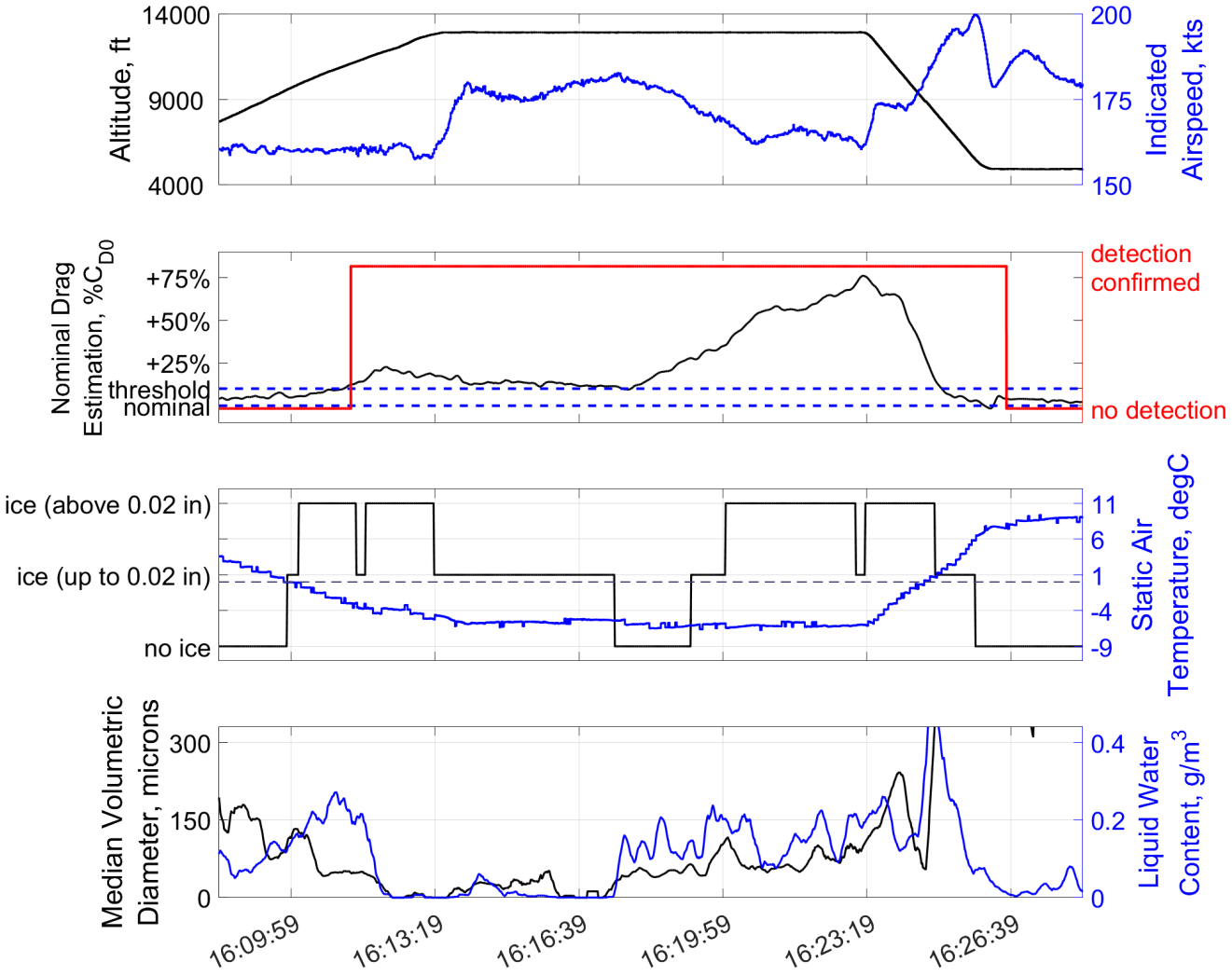

Fig. 30 Time history of IID system performance during specific encounter of the example flight on April 24th, 2023 (16:08:20 UTC to 16:28:20 UTC): altitude and indicated airspeed (top), nominal drag estimation and IID detection output (second plot), ice build-up on aircraft ice accretion sensor and static air temperature (dashed line 0 degC) (third plot), and MVD and LWC of encountered icing conditions (solid line) including the indication of the amount of SLD (dashed lines) (bottom), vertical zoom limiting plot to icing conditions neglecting rain above freezing point; updated detection threshold at 10 % relative drag increase.

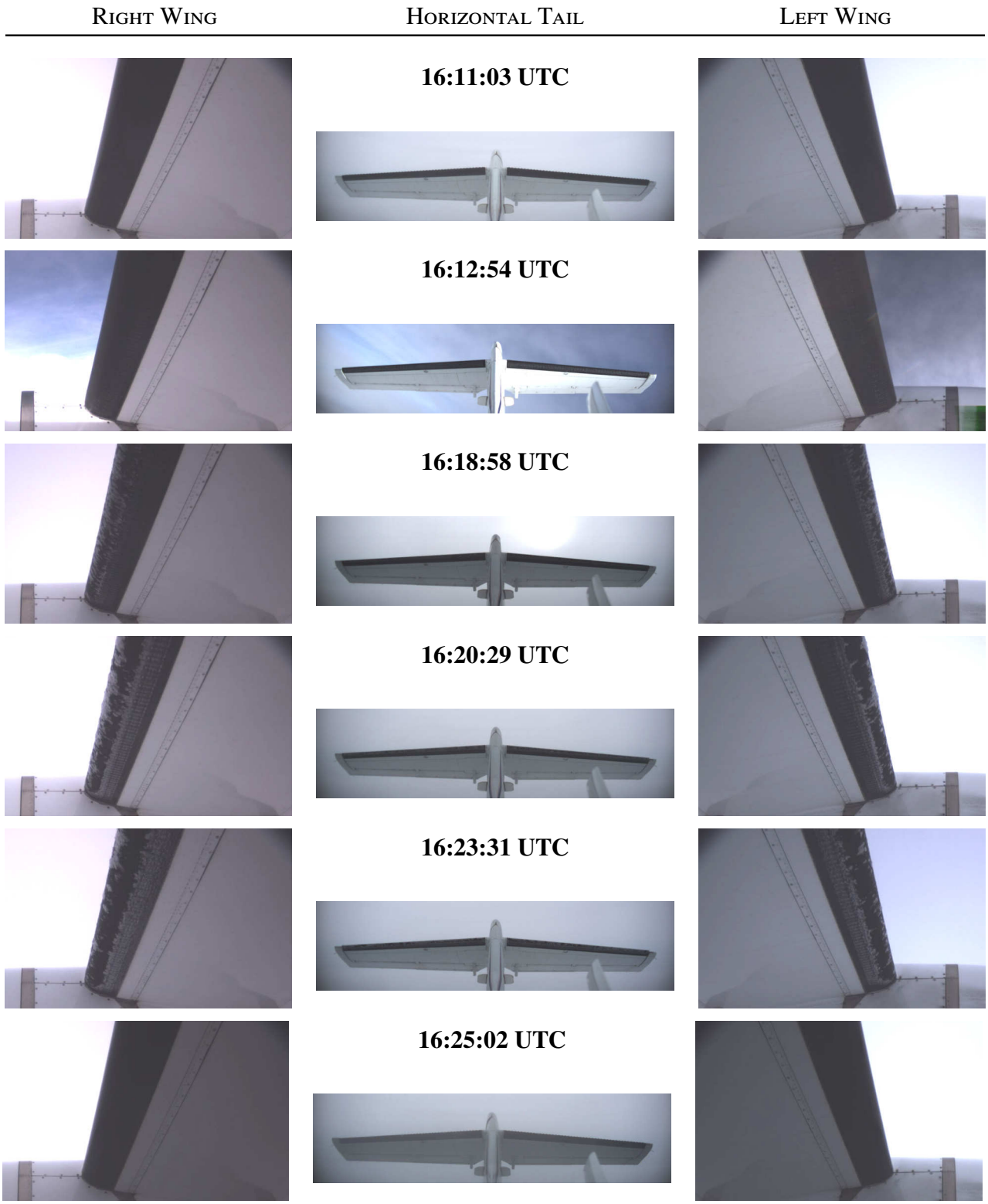

Fig. 31 Evolution of ice accretion on the airframe during icing encounter: camera views on left & right wing and horizontal tail for specific moments during flight (increased brightness and contrast); corresponding to encounter and IID detection given in Fig. 30; credit Safire / SENS4ICE project.

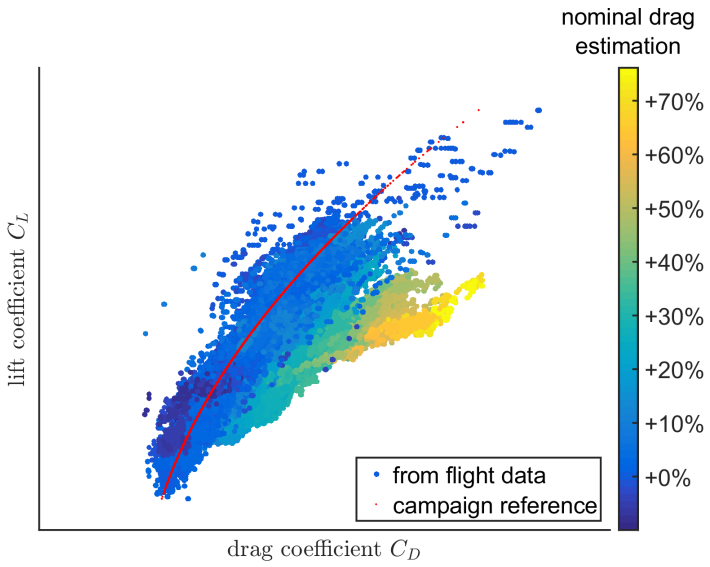

Fig. 32 Aircraft drag polar from example flight on April 24th, 2023: calculated lift and drag coefficient from flight data measurements and reference for the Safire ATR 42-320 with SENS4ICE modifications; drag coefficient data including the indication of nominal drag estimation calculated by IID.

5.2.2 Aerodynamic degradation due to icing

Figure 32 shows the aircraft lift and drag data (drag polar) calculated from the measured data for the whole flight (flaps retracted, gear up). For each data point available in the measurement, the lift and drag coefficient is calculated based on the available inertial and inflow measurements as well as the given engine thrust. The plot contains the aerodynamic reference used for the flight test reflecting the Safire ATR 42 characteristics with all SENS4ICE aircraft modifications (red line). The maximum degradation (large drag coefficients at medium lift coefficients, yellow and orange points) is correlated with a nominal drag estimation (change) of around 70 % (as given in the color bar on the right), but having 30 % to 40 % change in average (cyan points) related to icing in a more continuous manner, meaning that the degradation is to some extend saturated. This is also visible in the time history plots from this flight. Knowing that the main degradation is related to an increase of surface friction on (mainly) unprotected aircraft parts, this is reasonable.

Figure 33 contains the aircraft drag polar including an indication of the ice accretion announced by the aircraft ice accretion sensor. Overall, the drag increase (dots shifted to the right due to ice accretion) correspond well with the ice information given by the probe (cyan and yellow dots). But there are some blue dots in the shifted cloud indicating abnormal performance with is not directly correlated to the aircraft ice accretion sensor information. These are corresponding to the parts of the flight, where the performance was already or still degraded but the aircraft ice accretion sensor did not give any indication, as shown, e.g., in Fig. 28.

5.3 Comparison of presented results and initial conclusion

The two flights presented herein are conducted with different aircraft types under different conditions at different places of the world. Nevertheless, their results revealed valuable information about aircraft icing in general and more specifically the impact of different icing conditions (and resulting accumulations on the airframe) on the aircraft aerodynamics. Hence, the evaluation of this flight test data with regards to the IID performance gives some very good indications about the methods capabilities, advantages and limitations.

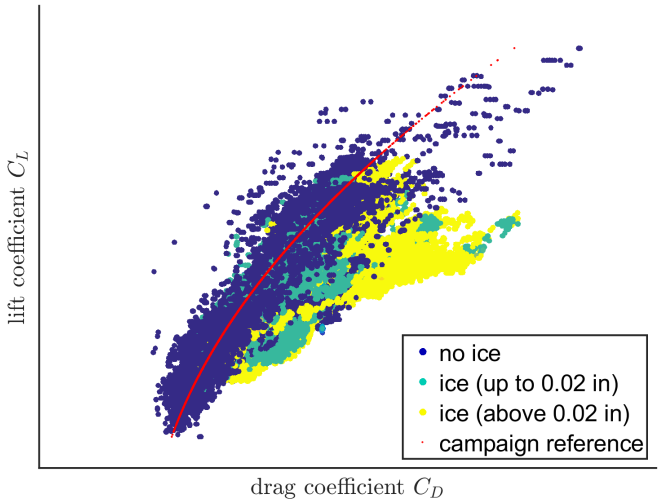

Fig. 33 Aircraft drag polar from example flight on April 24th, 2023: calculated lift and drag coefficient from flight data measurements and reference for the Safire ATR 42-320 with SENS4ICE modifications; drag coefficient data including the indication of ice accretion announced by aircraft ice accretion sensor.

For aircraft flight performance and aerodynamic degradation, the location, magnitude and type of ice accretion is relevant. The icing conditions encountered leading to these formations are only of secondary relevance from a more global point of view. Nevertheless, there is a strong correlation between conditions encountered and the resulting ice shapes, but also other effects like the impact of using a de-icing system. It was clearly shown in the time history plots presented herein, that the conditions itself neither indicate the presence or magnitude of the aerodynamic degradation nor further allow to classify it. In detail, encountered conditions with supercooled large droplets reveal similar aerodynamic effects as smaller drops, although in both cases the resulting shapes are also related to the amount of water in the air (LWC). For the aircraft operation, mainly the flight performance degradation and limitation of the safe operational envelope are of interest, which is supported by the IID during all the different example encounters from the campaigns.

The IID correctly and reliably indicates a performance degradation due to ice accretion if present. But, it is clearly visible in the time plots that the IID response time is in general much longer than any direct sensor response time, i.e. the aircraft ice accretion sensor from Safire. Nevertheless, the major output of the IID is the performance degradation which takes of course time to build up. After the degradation gets significant the IID indicates the threshold exceedance very fast according to the definition of the confirmation time. With reduction of the threshold (as shown in section 5.2 after the flight test campaign), the IID could be tuned in order to be more responsive to light ice accretion and therefore faster. Then, the IID would be more comparable to direct sensors, which could be interesting to specific applications where no direct sensing would be possible due to, e.g., payload restrictions. But this could also result in more false alarms if the threshold is below the limit of the expectable variation. During the European flight test campaign the 10 % threshold definition was a very good compromise and the IID response is well acceptable from a flight dynamics point of view.

Compared to the direct sensing output, the IID continuously monitors the flight performance. It also gives an indication of the present degradation if the current conditions are left. There had been several occasions during the European flight test campaign, where the aircraft left the clouds but was still degraded due to ice accretion on the airframe. During the US campaign, this was not observed because the aircraft was in stratiform clouds during the encounter. In both cases, as long as the aerodynamics are degraded, the IID output gives an indication, whereas, e.g., the aircraft ice accretion sensor and atmospheric measurements sometimes reset their indication while the airframe condition

has not changed and nominal performance was not restored. The IID is a continuous system which is permanently monitoring the aircraft flight performance characteristics.

This initial analysis of both flights presented here indicate that hybridization of dissimilar technologies, direct and indirect, might give a more comprehensive view on the icing situation and give additional relevant information to the pilots.

6 Summary and Conclusions

The SENS4ICE project is a big step towards successful and reliable detection of different icing conditions including SLD (Appendix O conditions). One key to achieve this goal is the indirect ice detection system based on an aircraft performance degradation, which provides several advantages compared to direct detection (ice sensors), which are mainly complementary. The IID provides e.g., retrofit capabilities, a simple software solution and a highly beneficial information about the remaining aircraft capabilities for safe aircraft operations. In addition, the indirect ice detection represents a second pillar for ice detection redundancy, when hybridized, and hence reduces the risk for common cause failures. It is based on the reliable measurements of the aircraft flight condition normally available in modern aircraft avionics.

The IID showed very good performance during both flight test campaigns. The IID was well capable of detecting the icing-related performance degradation and reliably monitor the corresponding drag increase. In addition, further modification made on the IID post-flight significantly enhanced the system performance by detecting flight performance degradations in a more sensitive and robust way. Nevertheless, the current version of the IID is an experimental system tailored to the specific flight test benches and their configurations during the SENS4ICE flight test campaigns (TRL5 after flight test campaign within the HIDS implementation). For an operational use within an in-service aircraft fleet, the algorithm must be further enhanced and implemented into the aircraft avionics, which was clearly not the scope of SENS4ICE. Although other direct ice measuring approaches for the detection of icing conditions or ice accretion on the airframe could deliver a partly similar information, the indirect detection using the performance monitoring approach would not require modifications of existing and future aircraft. Hence, the resulting information about the abnormal flight characteristics can then be used for controller adaptation to maintain within a safe flight envelope. Furthermore, the information from SENS4ICE about the (expectable) aerodynamic degradation due to different icing conditions might also support the development of robust flight control with special regard to future aerial vehicles.

The prototype running during the flight test campaigns was already designed to be highly adaptive to “known” changes of the aircraft flight performance, which was used to change the engine thrust representation in the IID for the Phenom 300 prototype. Also, the modification to the specific flight test bench prior to the flight test has proven the designed system flexibility. Hence, the system seems highly applicable to other transport aircraft or even any fixed-wing aircraft design with reasonable effort. Especially for smaller aircraft not equipped with direct ice detection technologies, the IID can be a valuable option for ice detection as a standalone system. In addition, the system might give a high potential for monitoring the aircraft icing status in terms of present ice accretion degrading the flight characteristics and the effectiveness of countermeasures (anti-ice and de-icing systems) trying to prevent any negative impact of icing on the aircraft operations, both for a standalone system or as part of the hybrid approach. Such an evaluation might be possible with the data available from SENS4ICE flight test, but was not in the specific scope of the project.

Disclaimer

The Phenom 300 flight test data analyzed is based on an experimental prototype. This aircraft prototype has embedded additional flight test instrumentation and features that do not represent any certified Phenom 300 aircraft model. Therefore, the analysis and performance estimations assessed in this study and within the SENS4ICE project do not represent the Phenom 300's certified performance.

Acknowledgments

The author wants to specially thank his colleague Falk Sachs for the contribution to this work of the IID development and flight test conduction. Within SENS4ICE the hybrid ice detection system was designed and developed by SAFRAN. Without this, the test of the IID during flight would not have been possible. The author wants to especially thank Annagrazia Orazzo and Bruno Thillays for their effort and support on the HIDS software development and hardware implementation on the flight test platforms. The author wants to further thank the SENS4ICE North America campaign flight test team for its structured and professional work to conduct the flight tests, especially Daniel Martins da Silva for coordinating with the SENS4ICE project group. In addition, the author wants to specially thank the SENS4ICE European campaign flight test team for its structured and professional work to conduct the flight tests even on very short notice according to the weather forecasts. A special thank goes to Tetyana Jiang (Safire) for the support with the flight test instrumentation, flight data and in-flight camera footage, and Jean-Philippe Desbios (Safire) for the campaign coordination.

Airborne data was obtained using the aircraft managed by Safire, the French facility for airborne research, an infrastructure of the French National Center for Scientific Research (CNRS), Météo-France and the French National Center for Space Studies (CNES). Distributed data are processed by SAFIRE.

Funding Information

The "SENSors and certifiable hybrid architectures for safer aviation in ICing Environment" (SENS4ICE) project has received funding from the European Union's Horizon 2020 research and innovation programme under grant agreement N° 824253.

References

[1] Steven D. Green. A study of u. s. inflight icing accidents and incidents, 1978 to 2002. Number AIAA 2006-82, Reno, Nevada, USA, January 9th - 12th, 2006. 44th AIAA Aerospace Sciences Meeting and Exhibit, American Institute of Aeronautics and Astronautics, Inc. (AIAA). DOI: 10.2514/6.2006-82.

[2] Steven D. Green. The icemaster database and an analysis of aircraft aerodynamic icing accidents and incidents. Technical Report DOT/FAA/TC-14/44, R1, Federal Aviation Administration, Atlantic City, NJ, USA, Oct. 2015.

[3] Anon. *Final Report (BFU 5X011-0/98)*. German Federal Bureau of Aircraft Accident Investigation, Braunschweig, Germany, April 2001.

[4] Anon. *Aircraft Accident Report (NTSB/AAR-96/01, DCA95MA001), Safety Board Report*. National Transportation Safety Board (NTSB), Washington, DC, USA, July 9th 1996.

[5] Christoph Deiler and Nicolas Fezans. Performance-based ice detection methodology. *Journal of Aircraft*, 57(2):209–223, March 2020. DOI: 10.2514/1.C034828.

[6] Christoph Deiler and Falk Sachs. Design and testing of an indirect ice detection methodology. Vienna, Austria, June 20th - 22nd 2023. SAE International Conference on Icing of Aircraft, Engines, and Structures, SAE International, Paper 2023-01-1493. DOI: 10.4271/2023-01-1493.

[7] Carsten W. Schwarz. The sens4ice eu project – sensors and certifiable hybrid architectures for safer aviation in icing environment – project overview and initial results. Stockholm, Sweden, September 4th - 9th 2022. 33th Congress of the International Council of the Aeronautical Sciences (ICAS). https://icas.org/ICAS_ARCHIVE/ICAS2020/data/papers/ICAS2022_0794_paper.pdf.

[8] Carsten W. Schwarz. Sens4ice eu project preliminary results. Vienna, Austria, June 20th - 22nd 2023. SAE International Conference on Icing of Aircraft, Engines, and Structures, SAE International, Paper 2023-01-1496.

[9] Christoph Deiler and Nicolas Fezans. Method and assistance system for detecting a degradation of flight performance, 2017. Patent Numbers: US11401044B2, EP3479181B1, WO2018002148A1, FR3053460B1, CA3029467A1, ES2919573T3.

[10] Christoph Deiler, Per Ohme, Christian Raab, Celso Mendonca, and Daniel Silva. Facing the challenges of supercooled large droplet icing: Results of a flight test based joint dlr-embraer research project. *SAE International Journal of Advances and Current Practices in Mobility*, 2(1):192–204, 2020. ISSN: 2641-9637. DOI: 10.4271/2019-01-1988.

[11] Christoph Deiler. Flight characteristics of iced aircraft. AIAA Scitech Forum, San Diego, California, USA, January 7th - 11th, 2019. American Institute of Aeronautics and Astronautics, Inc. (AIAA). DOI: 10.2514/6.2019-0560.

[12] Christoph Deiler and Thomas Kilian. Dynamic aircraft simulation model covering local icing effects. *CEAS Aeronautical Journal*, March 2018. DOI: 10.1007/s13272-018-0291-6.

[13] Christoph Deiler. Aerodynamic modeling, system identification, and analysis of iced aircraft configurations. *Journal of Aircraft*, 55(1):145–161, January-February 2018. DOI: 10.2514/1.C034390.

[14] Tina Jurkat-Witschas, Johannes Lucke, Carsten W. Schwarz, Christoph Deiler, Falk Sachs, Simon Kirschler, Deniz Menekay, Christiane Voigt, Ben Bernstein, Olivier Jaron, Frank Kalinka, Alessandra Zollo, Lyle Lilie, Johanna Mayer, Christian Page, Benoit Vié, Aurelien Bourdon, Rogerio Pereira Lima, and Luiz Vieira. Overview of cloud microphysical measurements during the sens4ice airborne test campaigns: Contrasting icing frequencies from climatological data to first results from airborne observations. Vienna, Austria, June 20th - 22nd 2023. SAE International Conference on Icing of Aircraft, Engines, and Structures, SAE International, Paper 2023-01-1491.

[15] Thomas Lombaerts, Stefan Schuet, Diana Acosta, John Kaneshige, and Lynne Martin. Piloted simulator evaluation of maneuvering envelope information for flight crew awareness. Number AIAA 2015-1546 in AIAA SciTech - AIAA Guidance, Navigation, and Control Conference, Kissimmee, Florida, USA, January 5th - 9th 2015. American Institute of Aeronautics and Astronautics, Inc. (AIAA). DOI: 10.2514/6.2015-1546.

[16] Anon. Ice accretion simulation. AGARD Advisory Report 344, Advisory Group for Aerospace Research & Development (AGARD) - Fluid Dynamics Panel Working Group 20, North Atlantic Treaty Organization (NATO), Neuilly-Sur-Seine, France, December 1997.

[17] Michael B. Bragg, William R. Perkins, Nadine B. Sarter, Tamer Başar, Petros G. Voulgaris, Holly M. Gurbacki, James W. Melody, and Scott A. McCray. An interdisciplinary approach to inflight aircraft icing safety. Number AIAA 98-0095, Reno, Nevada, USA, January 12th-15th 1998. 36th AIAA Aerospace Sciences Meeting and Exhibit, American Institute of Aeronautics and Astronautics, Inc. (AIAA). DOI: 10.2514/6.1998-95.

[18] Thomas T. Myers, David H. Klyde, and Raymond E. Magdaleno. The dynamic icing detection system (dids). Reno, Nevada, USA, January 10th - 13th, 1999. 38th AIAA Aerospace Sciences Meeting and Exhibit, American Institute of Aeronautics and Astronautics, Inc. (AIAA). DOI: 10.2514/6.2000-364.

[19] James W. Melody, Tamer Başar, William R. Perkins, and Petros G. Voulgaris. Parameter identification for inflight detection and characterization of aircraft icing. *Control Engineering Practice*, 8(9):985–1001, September 2000. DOI: 10.1016/S0967-0661(00)00046-0.

[20] Michael B. Bragg, Tamer Başar, William R. Perkins, Michael S. Selig, Petros G. Voulgaris, James W. Melody, and Nadine B. Sater. Smart icing systems for aircraft icing safety. Reno, Nevada, USA, January 14th - 17th 2002. 40th AIAA Aerospace Sciences Meeting and Exhibit, American Institute of Aeronautics and Astronautics, Inc. (AIAA). DOI: 10.2514/6.2002-813.

[21] Rahmi Aykan, Chingiz Hajiyev, and Fikret Caliskan. Aircraft icing detection, identification and reconfigurable control based on kalman filtering and neural networks. San Francisco, California, USA, August 15th - 18th 2005. AIAA Atmospheric Flight Mechanics Conference and Exhibit, American Institute of Aeronautics and Astronautics, Inc. (AIAA). DOI: 10.2514/6.2005-6220.

[22] David R. Gingras, Billy P. Barnhart, Richard J. Ranuado, Thomas P. Ratvasky, and Eugene A. Morelli. Envelope protection for in-flight ice contamination. Orlando, Florida, USA, January 5th - 8th, 2009. 47th Aerospace Sciences Meeting, American Institute of Aeronautics and Astronautics, Inc. (AIAA). DOI: 10.2514/6.2009-1458.

[23] Christoph Deiler. Evaluation of aircraft performance variation during daily flight operations. Friedrichshafen, Germany, Sept. 2018. Deutscher Luft- und Raumfahrtkongress, Deutsche Gesellschaft fur Luft- und Raumfahrt (DGLR). DOI: 10.25967/480025.

[24] Christoph Deiler. Aerodynamic model adjustment for an accurate flight performance representation using a large operational flight data base. *CEAS Aeronautical Journal*, 14(2):527–538, Mar. 2023. DOI: 10.1007/s13272-023-00659-w.

[25] Christoph Deiler. Testing of an indirect ice detection methodology in the Horizon2020 project SENS4ICE. Stuttgart, Germany, September 19th-21st 2023. Deutscher Luft- und Raumfahrtkongress, Deutsche Gesellschaft fur Luft- und Raumfahrt (DGLR). `https://elib.dlr.de/197520/`.

[26] Christoph Deiler. Performance-based ice detection first results from SENS4ICE european flight test campaign. Orlando, Florida, USA, January 2024. AIAA Scitech Forum, American Institute of Aeronautics and Astronautics, Inc. (AIAA). DOI: 10.2514/6.2024-2817.

[27] Annagrazia Orazzo, Bruno Thillays, and Christoph Deiler. Final report on hybrid ice detection development. SENS4ICE Deliverable D4.2, SAFRAN Aerosystems & DLR, February 06th 2024. `https://www.sens4ice-project.eu/sites/sens4ice/files/media/2024-02/SENS4ICE_D4.2_Final_report_on_HIDS_development_Safran_20240201.pdf`.